生物奈米馬達

中原大學 生物科技學系

吳宗遠

微小機械與細胞

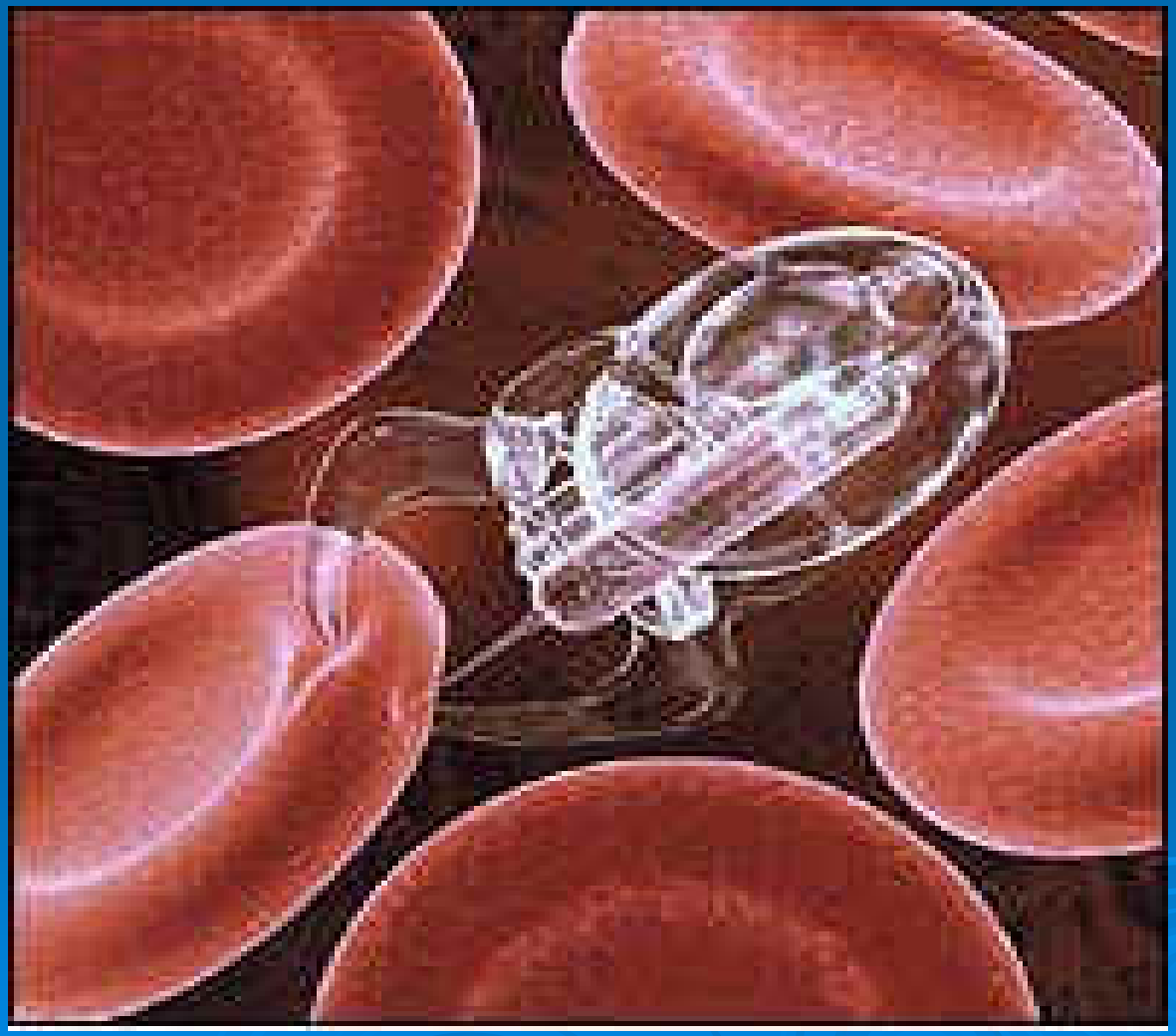

Virus---self replicated particles (**machine**)

(奈米獵殺)

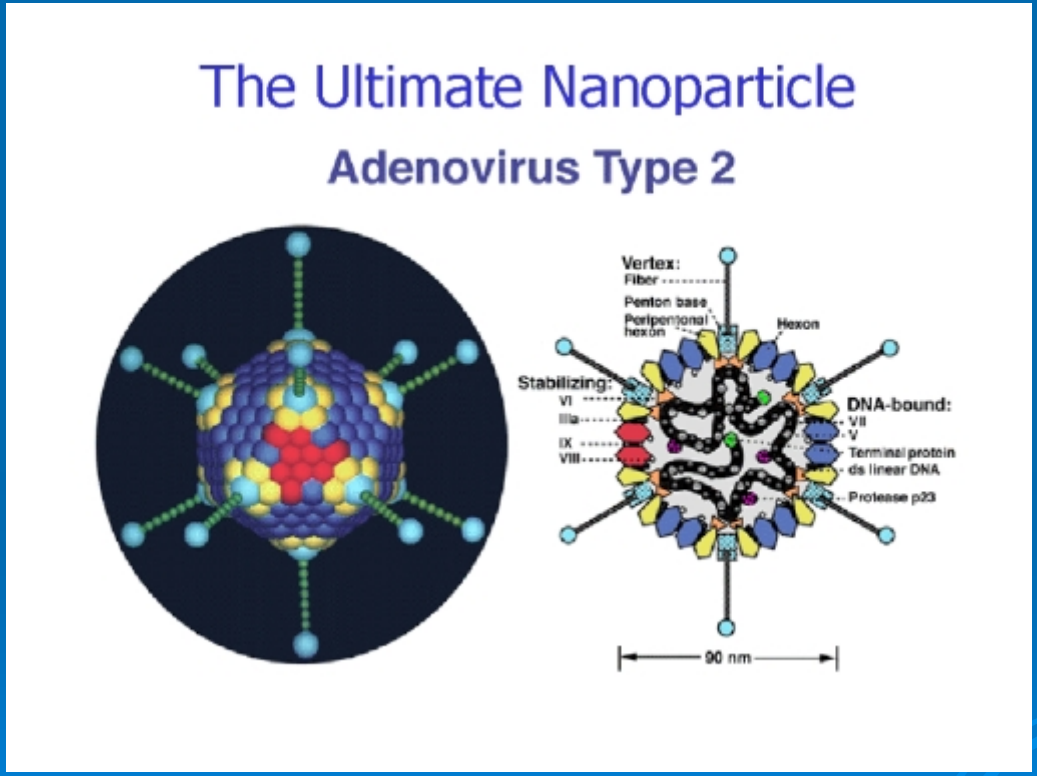

Virus: proteins plus nucleic acids (DNA or RNA)

The self replicated **nanomachine**

DNA 奈米電線—Biological Template approach

9. Lipowitz, J., Rabe, J. A., Nguyen, K. T., Orr, L. D. & Androl, R. R. Structure and properties of polymer-derived stoichiometric SiC fiber. *Ceram. Eng. Sci. Proc.* **16**, 55–62 (1995).
10. Bocker, W., Landfermann, H. & Hausner, H. Sintering of alpha silicon carbide with additions of aluminium. *Powder Metall. Int.* **11**, 83–85 (1979).
11. Alliegro, R. A., Coffin, L. B. & Tinklepaugh, J. R. Pressure-sintered silicon carbide. *J. Am. Ceram. Soc.* **39**, 386–389 (1956).
12. Izeki, T. in *Handbook of Corrosion Resistance of Ceramics* (ed. Izeki, T.) 61–67 (Kyoritsu Syuppan, Tokyo, 1985).
13. Takeda, M. & Imai, Y. in *Proc. 7th Symp. on High-Performance Materials for Severe Environments* 227–234 (R&D Inst. of Metals and Composites for Future Industries, Tokyo, 1996).

Acknowledgements. We thank Y. Harada, H. Yamaoka, T. Hisayuki, S. Iwase and T. Fujii for their contributions.

Correspondence and requests for materials should be addressed to T.I. (e-mail: 24613u@ube-ind.co.jp)

DNA-templated assembly and electrode attachment of a conducting silver wire

Erez Braun*, Yoav Eichen†‡, Uri Sivan*‡ & Gdalyahu Ben-Yoseph*‡

** Department of Physics, † Department of Chemistry, ‡ Solid State Institute, Technion-Israel Institute of Technology, Haifa 32000, Israel*

Recent research in the field of nanometre-scale electronics has focused on two fundamental issues: the operating principles of small-scale devices, and schemes that lead to their realization and eventual integration into useful circuits. Experimental studies on molecular[1] to submicrometre[2] quantum dots and on the electrical transport in carbon nanotubes[3–5] have confirmed theoretical predictions[6–8] of an increasing role for charging effects as the device size diminishes. Nevertheless, the construction of nanometre-scale circuits from such devices remains problematic, largely owing to the difficulties of achieving inter-element wiring and electrical interfacing to macroscopic electrodes. The use of molecular recognition processes and the self-assembly of molecules into supramolecular structures[9,10] might help overcome these difficulties. In this context, DNA has the appropriate molecular-recognition[11] and mechanical[12–16] properties, but poor electrical characteristics prevent its direct use in electrical circuits. Here we describe a two-step procedure that may allow the application of DNA to the construction of functional circuits. In our scheme, hybridization of the DNA molecule with surface-bound oligonucleotides is first used to stretch it between two gold electrodes; the DNA molecule is then used as a template for the vectorial growth of a 12 μm long, 100 nm wide conductive silver wire. The experiment confirms that the recognition capabilities of DNA can be exploited for the targeted attachment of functional wires.

The first step in the construction of the silver wire involves the self-assembly of a DNA template connecting two gold electrodes 12–16 μm apart (see Fig. 1 for an outline of the procedure). First, 12-base oligonucleotides, derivatized with a disulphide group at their 3′ end, are attached to the electrodes through sulphur–gold interactions. The electrodes are each marked with specific but different oligonucleotide sequences. A connection is then made by hybridizing two distant surface-bound oligonucleotides with a 16 μm long and fluorescently labelled λ-DNA that contains two 12-base sticky ends, where each of the ends is complementary to one of the two different sequences attached to the gold electrodes. Hybridization on both ends is facilitated by covering the electrodes with an aqueous solution containing the λ-DNA and inducing a flow perpendicular to the electrodes, thereby stretching the λ-DNA molecules in the flow direction (other stretching methods can be used; for application of an electric field, see ref. 17). The flow is terminated when a single DNA bridge is observed by fluorescence microscopy (see Fig. 2), usually after a few minutes. Curving of the DNA bridge under a flow parallel to the electrodes shows it to be attached solely to the electrodes. The method does not guarantee a single DNA bridge. However, *in situ* video microscopy and imaging of the resulting silver wire by atomic force microscopy (AFM; see below) reveal a silver bridge only in places where DNA was previously fluorescently imaged. We also tried stretching the DNA between two electrodes in the reverse order, performing hybridization and ligation of the disulphide-derivatized oligonucleotides to the long DNA molecule before it was applied to the sample (see Methods section). The binding of the derivatized λ-DNA in this case was again aided by an induced perpendicular flow. Both methods work equally well.

To instill electrical functionality, silver metal is vectorially deposited along the DNA molecule. The three-step chemical deposition process (see Fig. 1 and Methods) is based on selective localization of silver ions along the DNA through Ag^+/Na^+ ion-exchange[18] and formation of complexes between the silver and the DNA bases[19–21]. The Ag^+/Na^+ ion-exchange process is monitored by following the almost instantaneous quenching of the fluorescence signal of the labelled DNA. The ion-exchange process, which is highly selective and restricted to the DNA template only, is terminated when the fluorescence signal drops to 1–5% of its initial value (the quenching is much faster than normal bleaching of the fluorescent dye). The silver ion-exchanged DNA is then reduced to form nanometre-sized metallic silver aggregates bound to the DNA skeleton. These silver aggregates are subsequently further 'developed', much as in the standard photographic procedure, using an acidic solution of hydroquinone and silver ions under low light conditions[22,23]. Such

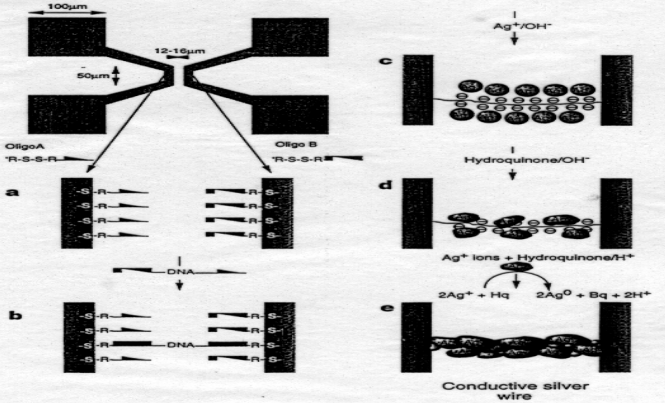

Figure 1 Construction of a silver wire connecting two gold electrodes. The top left image shows the electrode pattern (0.5 × 0.5 mm) used in the experiments. The two 50 μm long, parallel electrodes are connected to four (100 × 100 μm) bonding pads. **a**, Oligonucleotides with two different sequences attached to the electrodes. **b**, λ-DNA bridge connecting the two electrodes. **c**, Silver-ion-loaded DNA bridge. **d**, Metallic silver aggregates bound to the DNA skeleton. **e**, Fully developed silver wire. A full description of the preparation steps can be found in the Methods section.

The man who dare to think small

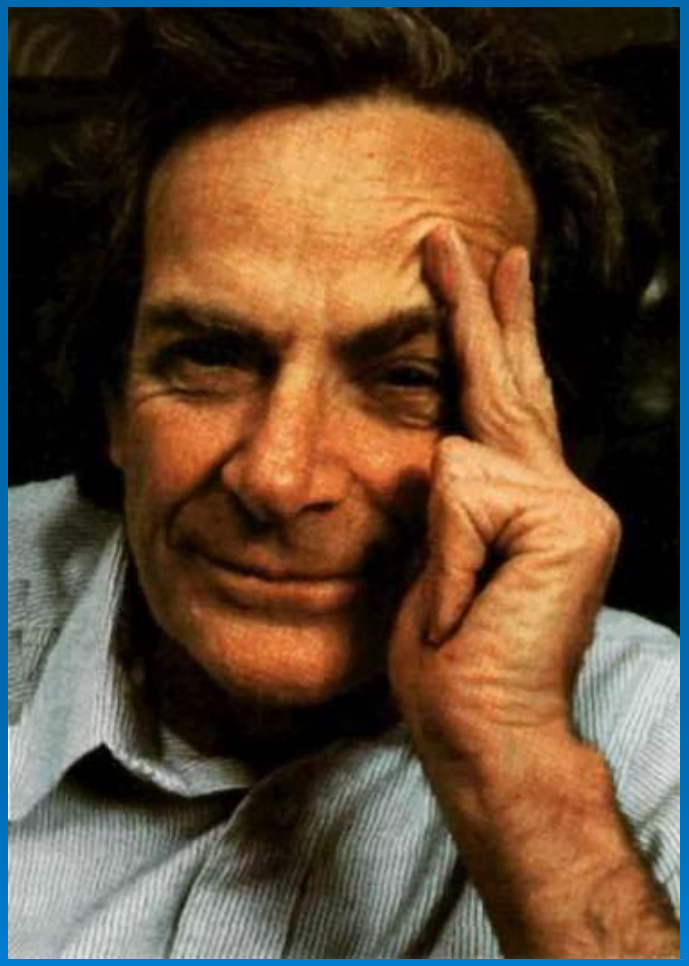

Small is beautiful !

徐志摩 (1897-1931)

Large is beautiful !

The New Biochemistry: Macromolecular Machines

1998 Welch Conference, Houston, TX, October 26 & 27, 1998

Joseph L. Goldstein, Program Chairman

Machines That Control Cell Division

Ira Herskowitz – Discussion Leader

- Robert Weinberg – Oncogenes and Tumor Suppressors
- Steve Elledge – Cyclin Kinase Complexes
- Nikola Pavletich – Cell Cycle Regulatory Proteins
- Robert Huber – Proteasome

Machines That Produce DNA, RNA, and Protein

Steve McKnight – Discussion Leader

- Mike O'Donnell – DNA Replicase
- Tom Cech – Telomerase
- Robert Tjian – Basal Transcription Complex
- Cynthia Wolberger – Multimeric DNA-Binding Proteins

Machines That Transduce Signals

Susan Taylor – Discussion Leader

- Tony Pawson – Protein Modules
- Al Gilman – Heterotrimeric G Proteins
- Pierre Chambon – Nuclear Receptor Superfamily
- Michael Brown – SREBP Pathway

Machines That Move Molecules

Hans Deisenhofer – Discussion Leader

- Ulrich Hartl – Molecular Chaperones
- Peter Walter – Unfolded Protein Response Pathway
- Rod McKinnon – Ion Channels
- Thomas Südhof – Synaptic Vesicle Cycle

奈米馬達的最適材料可能是蛋白質 (protein)

WHY?

Molecular Motors

linear motion motor

Rotatory motion motor

All this molecular motor in the cell are protein molecules

What is the energy source?

Chemical energy convert to mechanical energy

Linear molecular motors: track dependent

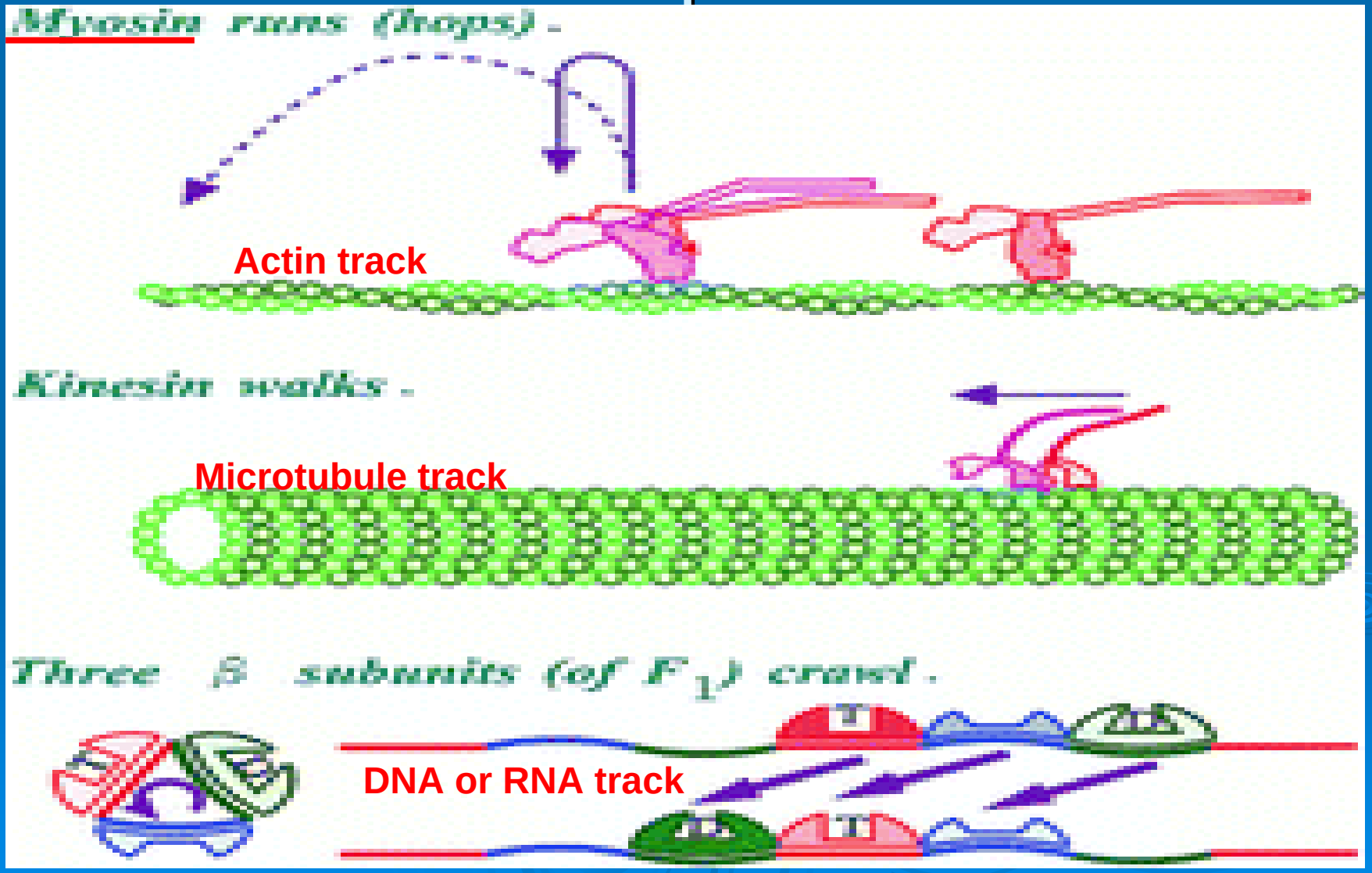

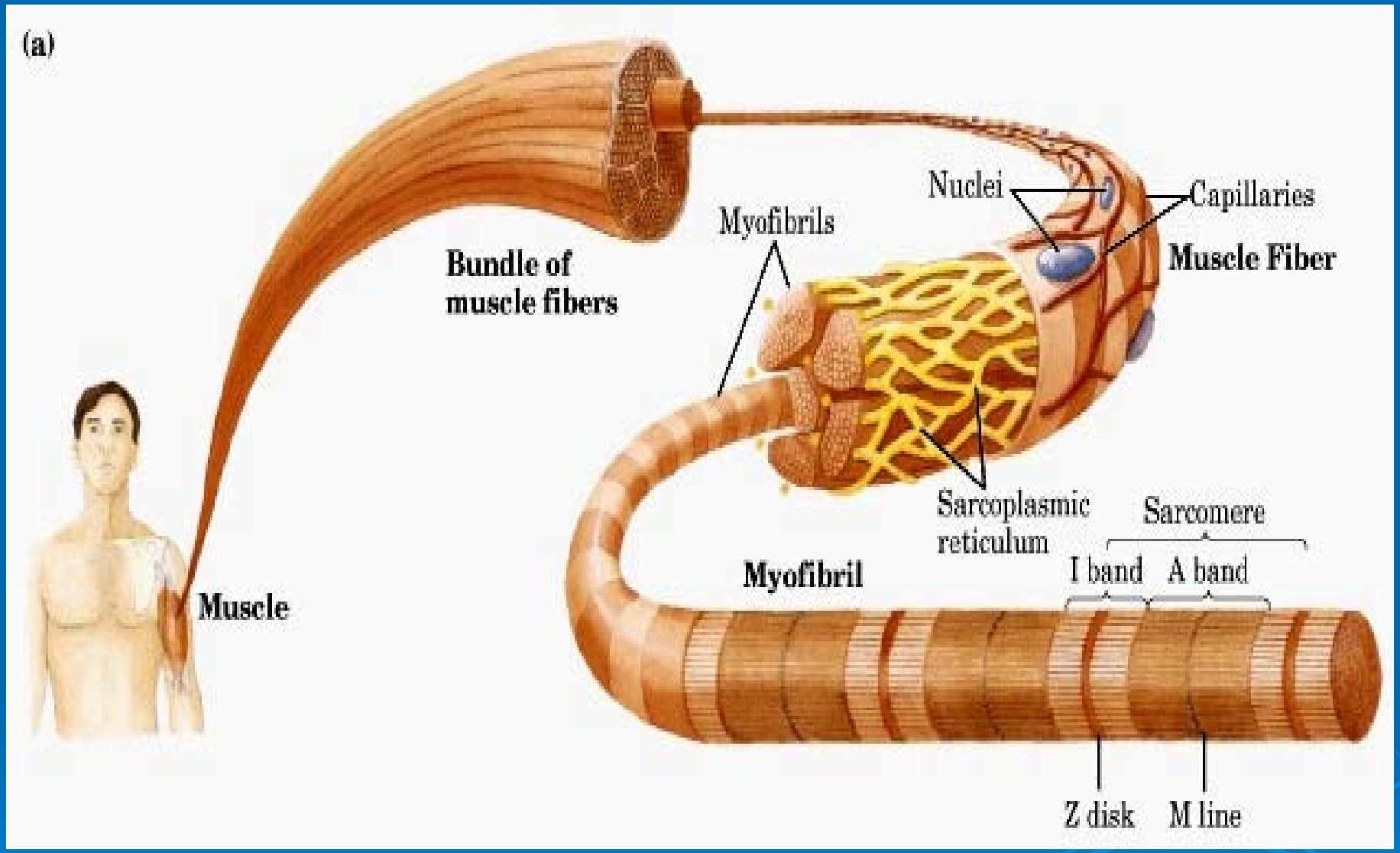

Figure 7-31 (a) Structure of skeletal muscle. Muscle fibers consist of single, elongated, multinucleated cells that arise from the fusion of many precursor cells.

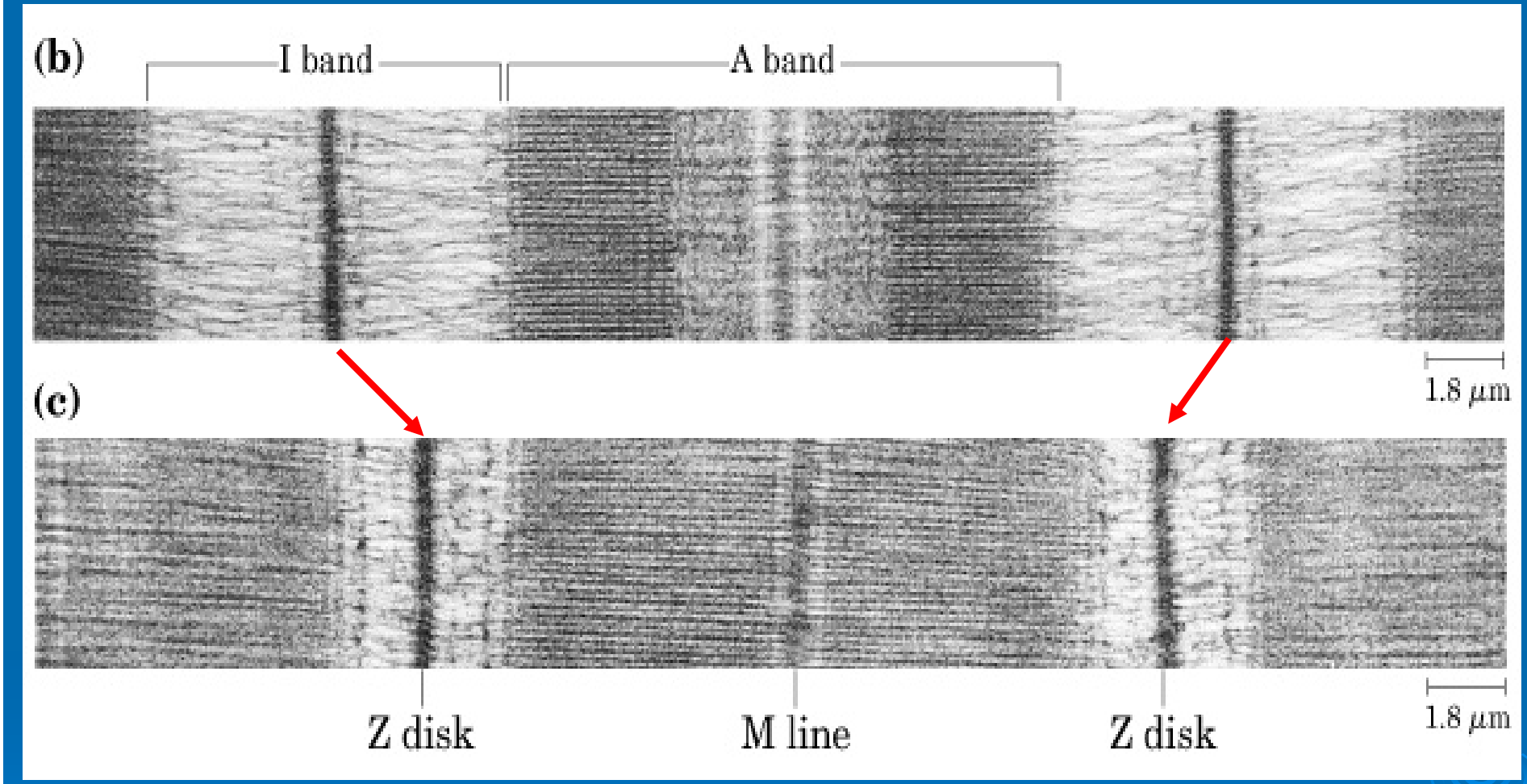

Figure 7-31 (b)、(c) Structure of skeletal muscle.

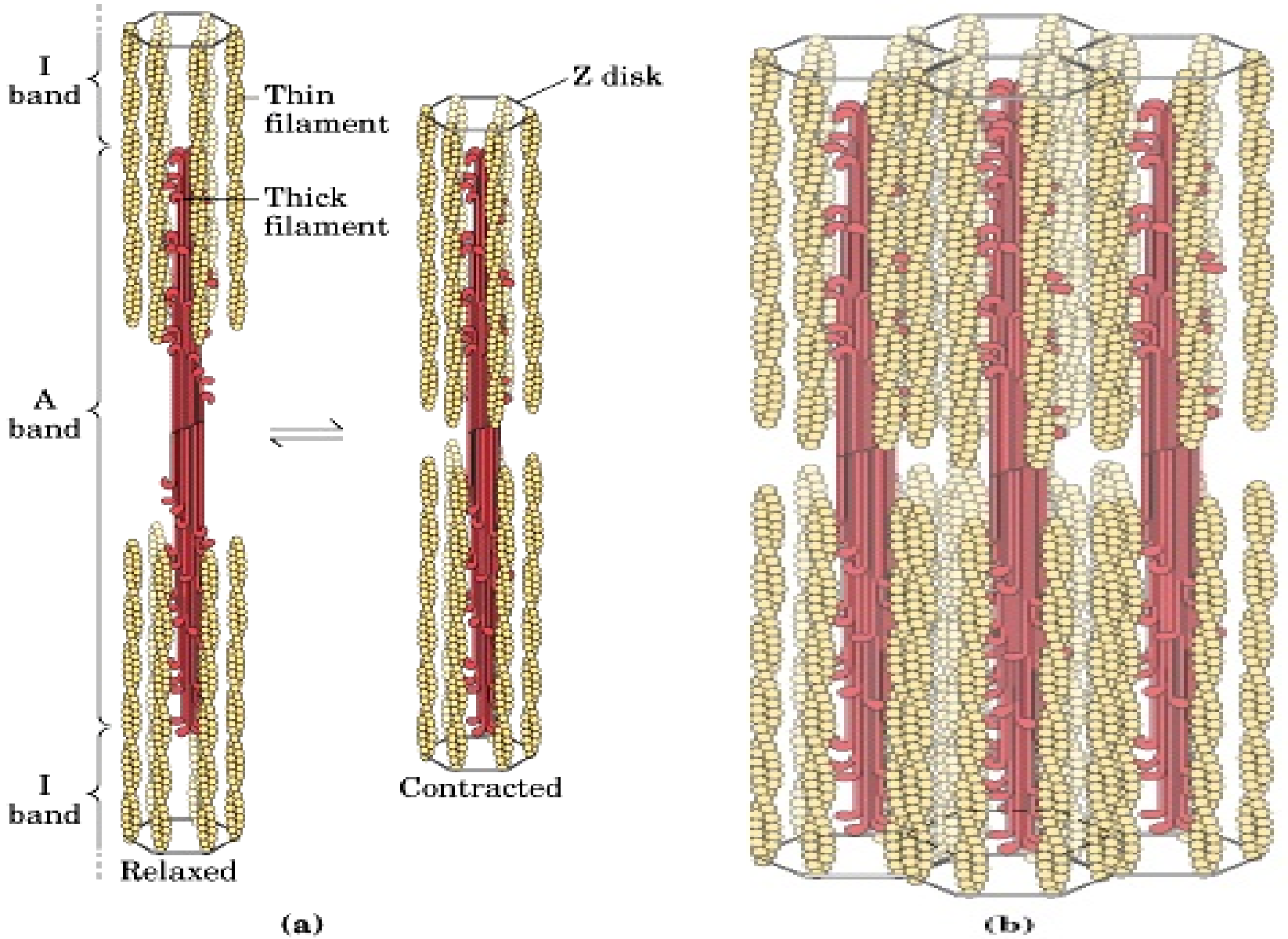

Figure 7-32 (a) Muscle contraction.

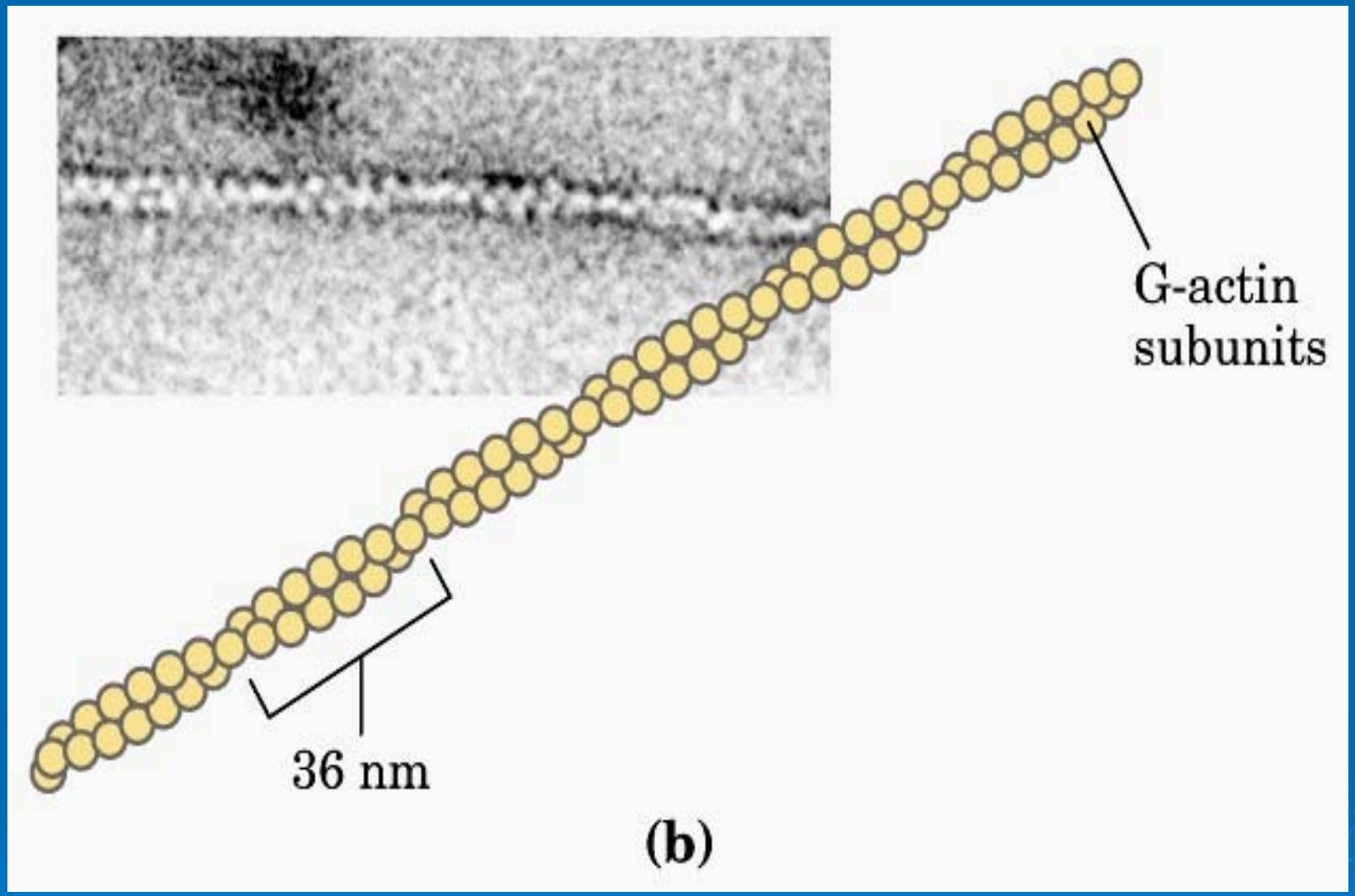

Figure 7-30 (b) The major components of muscle. F-actin.

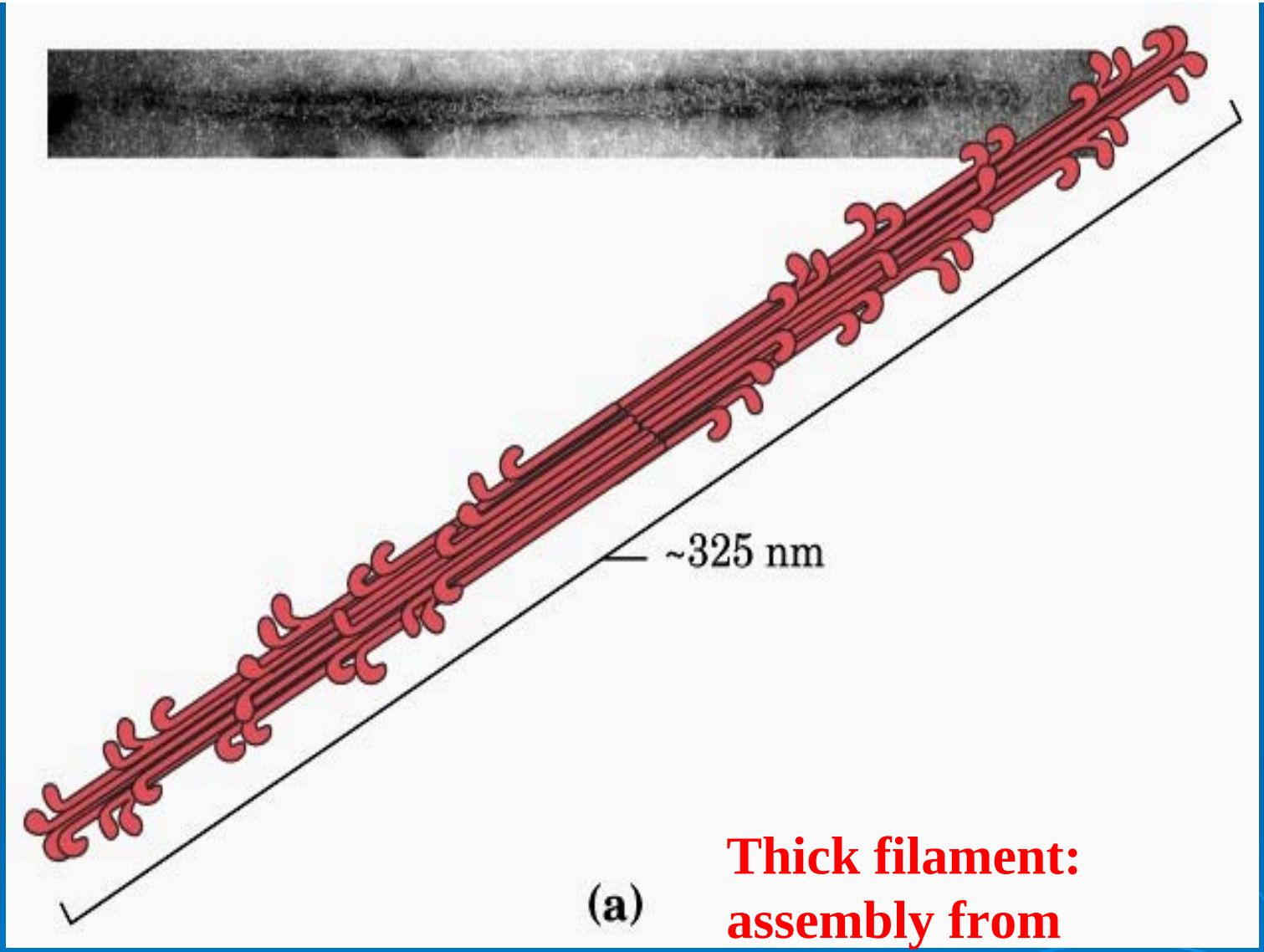

Thick filament: assembly from myosin

Figure 7-30 (a) The major components of muscle.
thick filament

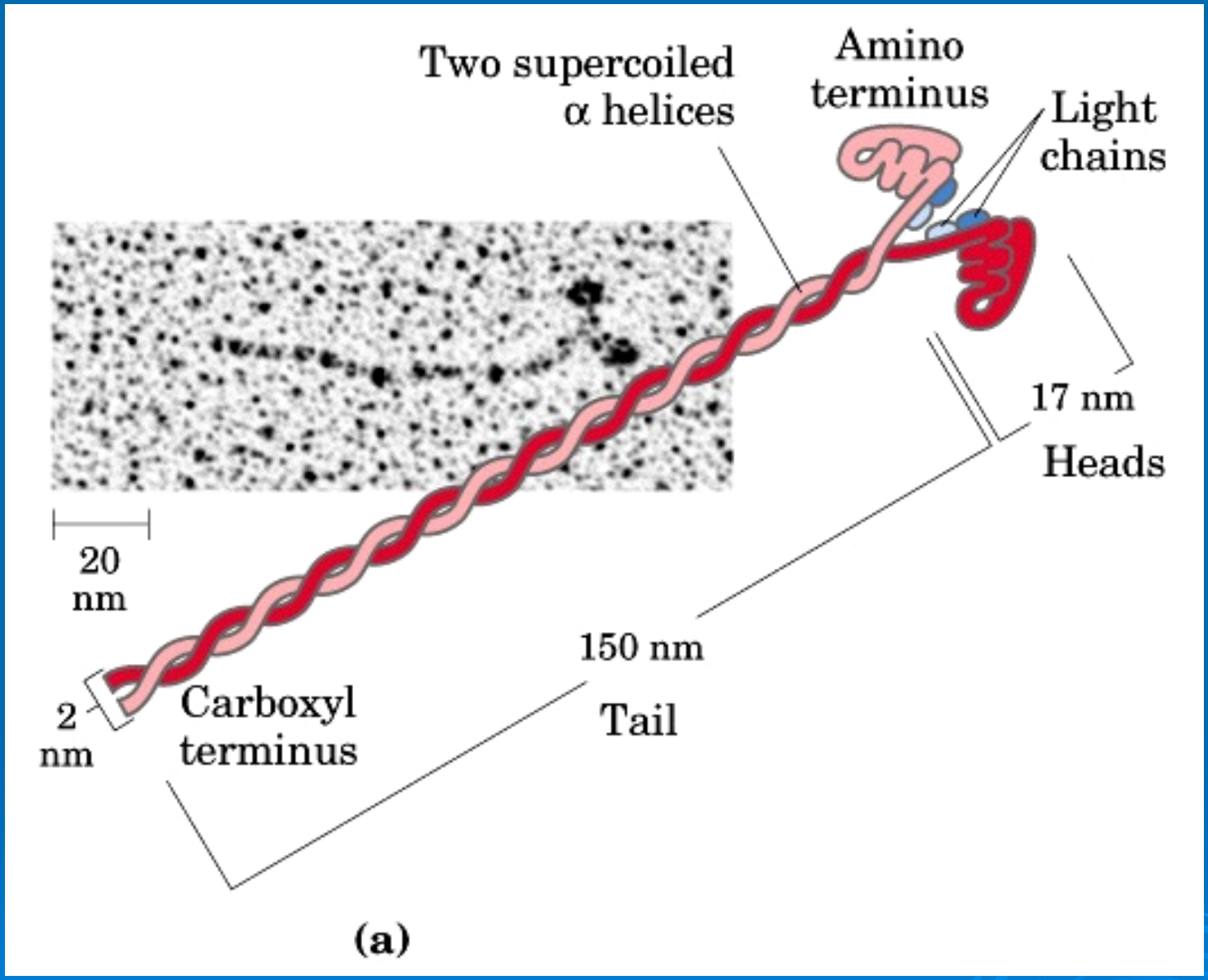

Figure 7-29 (a) Myosin. Two heavy chain.

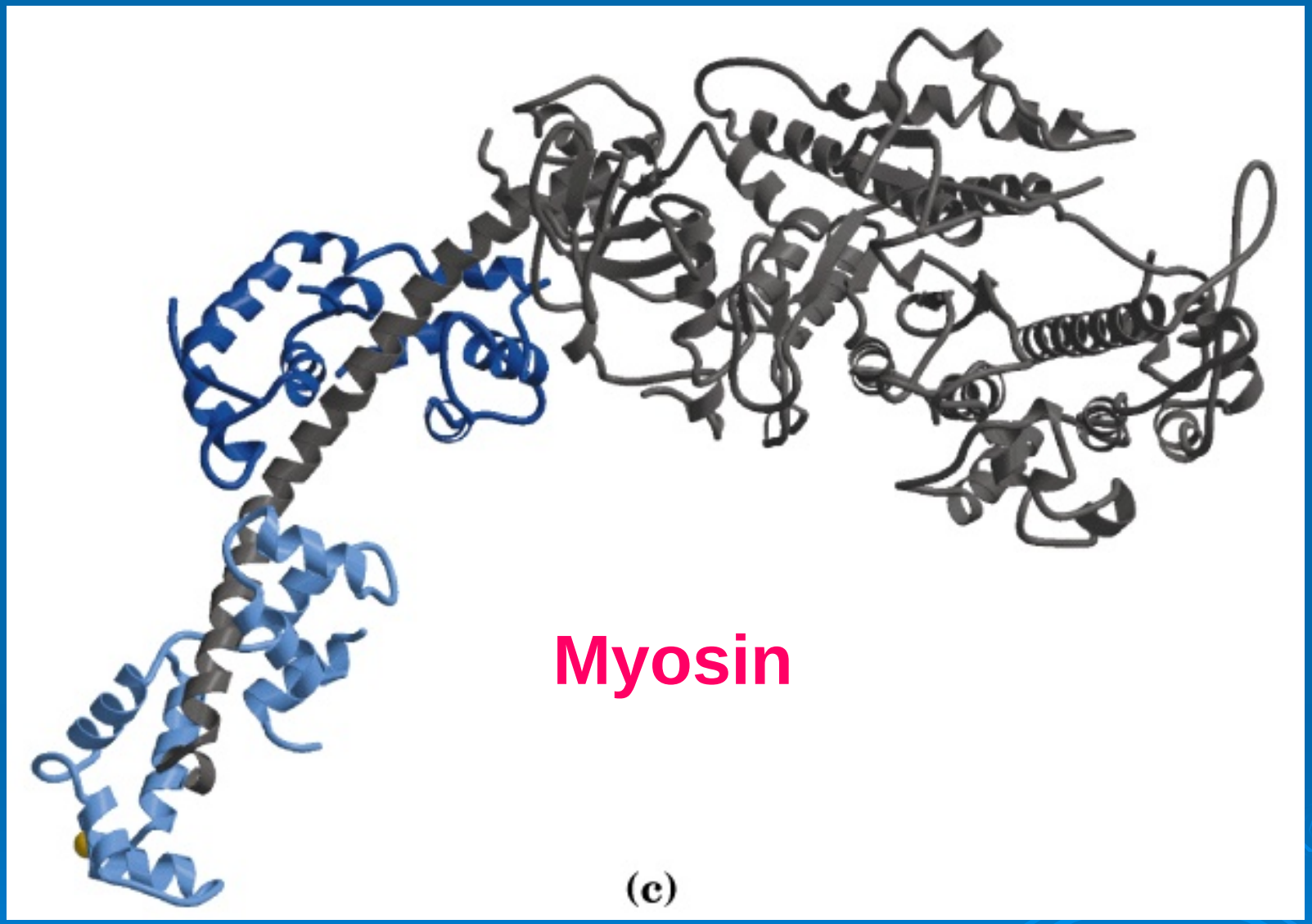

Figure 7-29 (c) Myosin. Ribbon representation of the myosin S1 fragment.

Kinesin/dynein

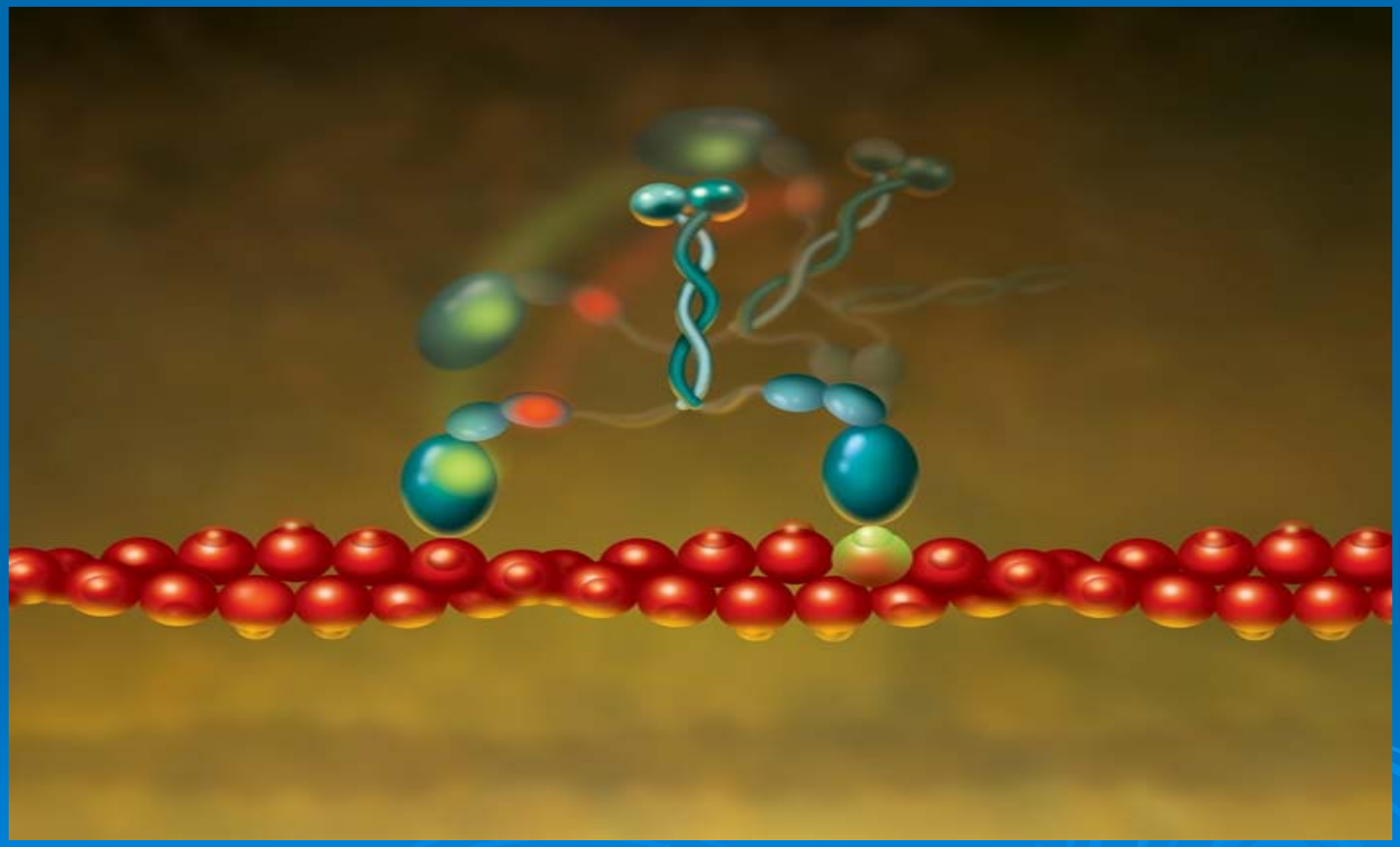

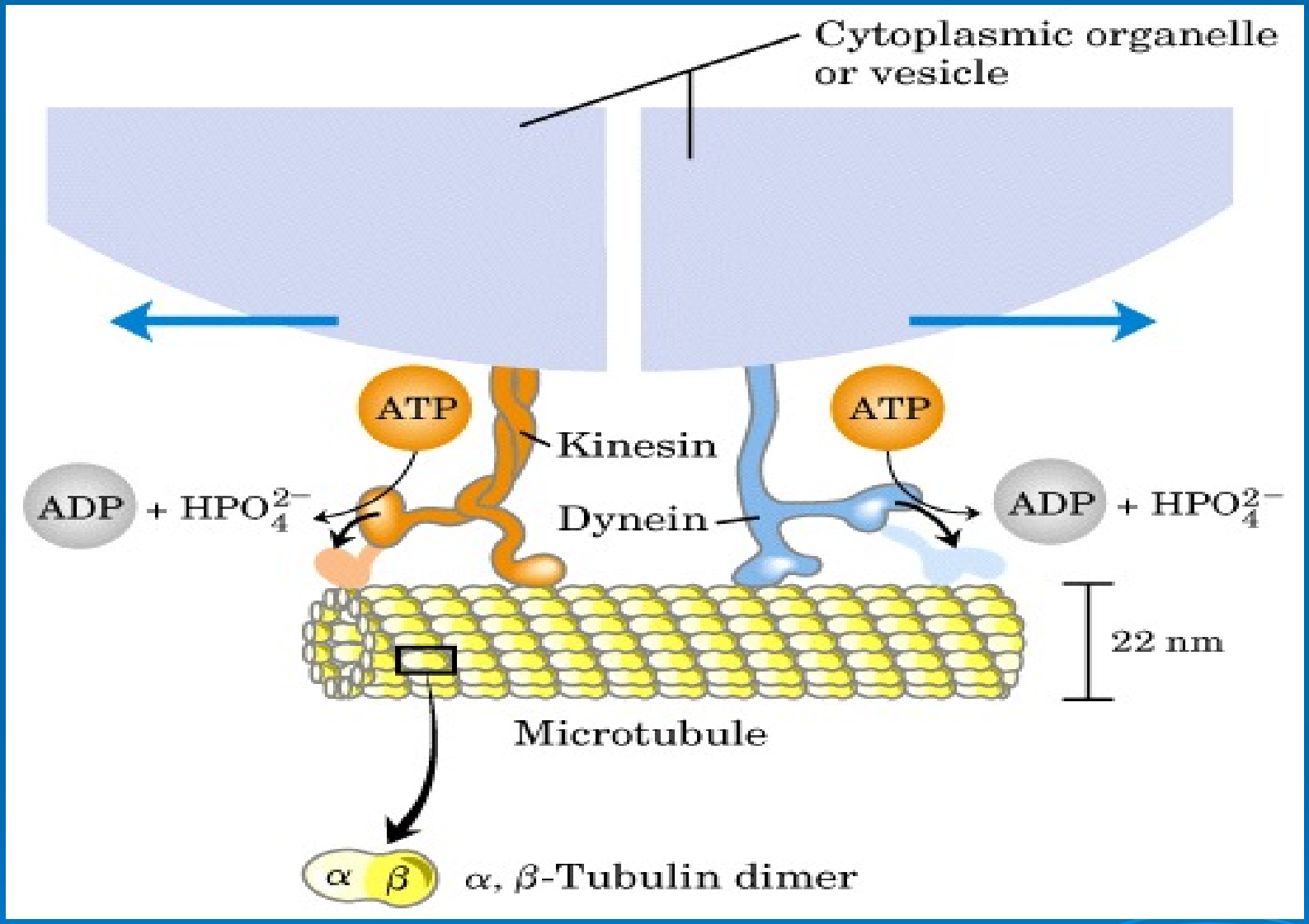

Figure 2-19 : Kinesin and cytoplasmic dynein are ATP-driven molecular motors that can attach to cytoplasmic organelles or vesicles and drag along microtubular "rails" at a rate of about 1 um/s.

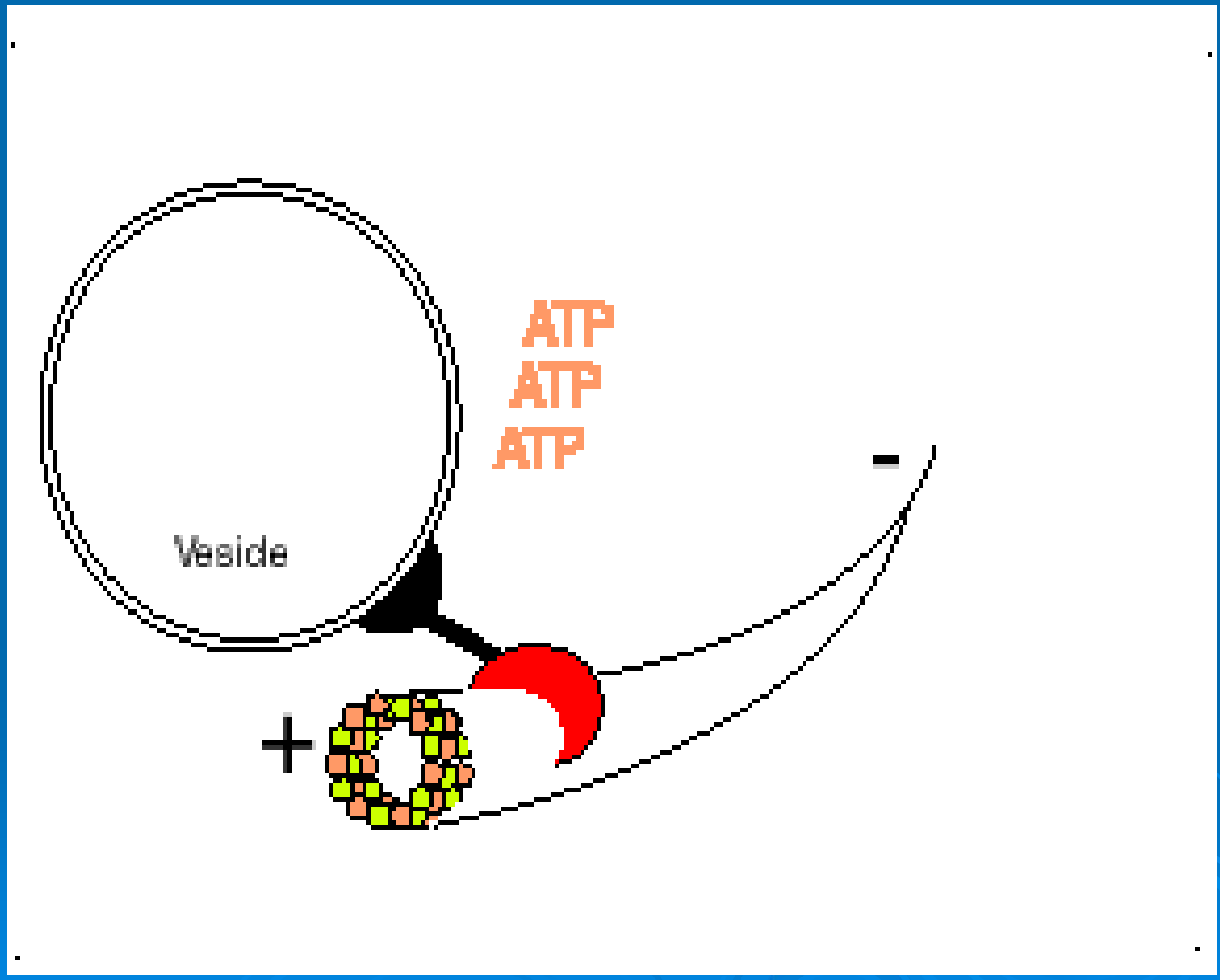
ATP
ATP
ATP
Vesicle
-
+

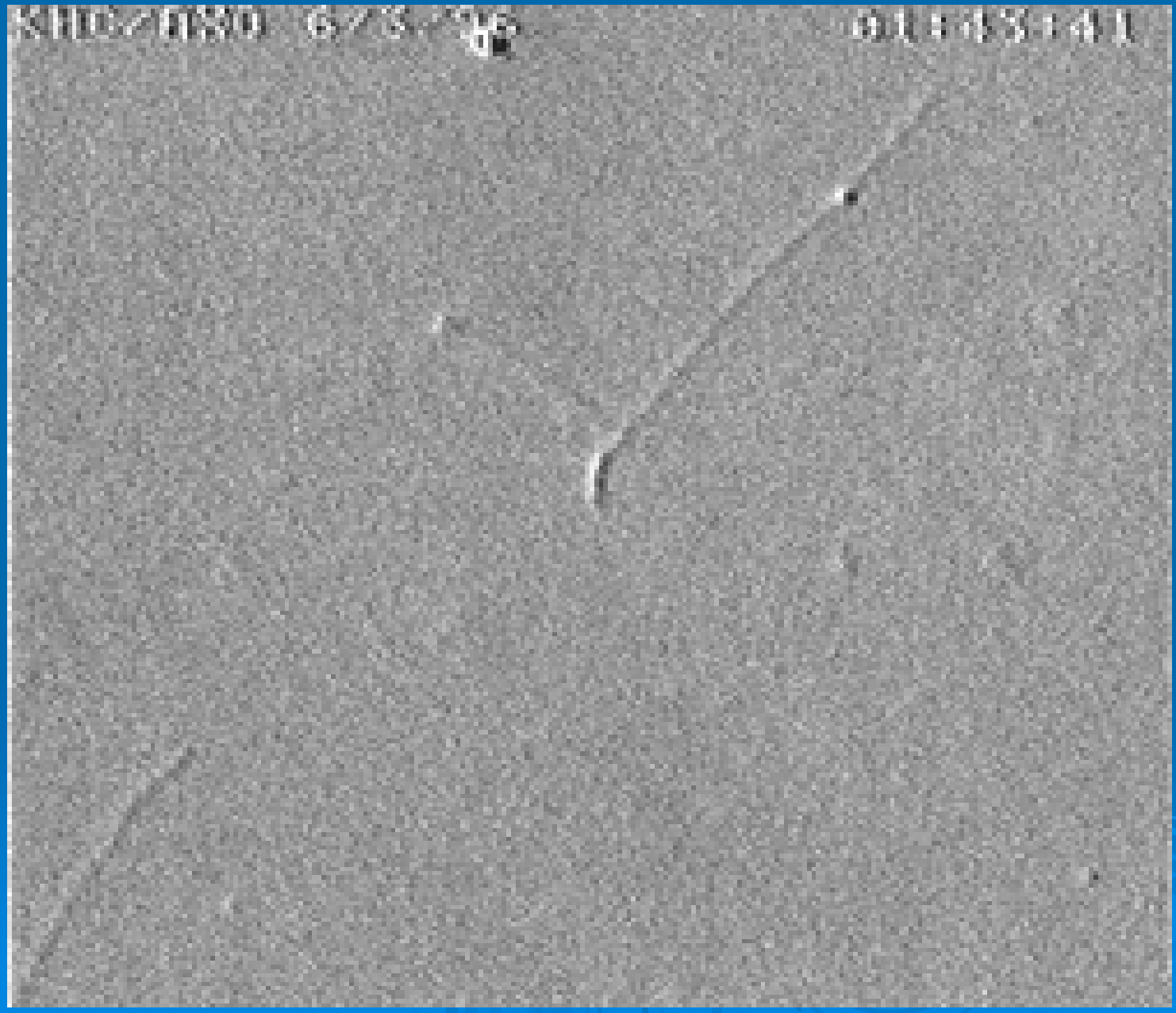

MATERIALS SCIENCE

Toward Devices Powered by Biomolecular Motors

Biomolecular motors can be used in nanometer-scale devices to perform mechanical work. This approach will assist the development of active nanostructures.

Nanofluidics with molecular motors. In van den Heuvel *et al.*'s work (*2*), an electric field is used to steer the microtubules into one of two arms of a Y junction; the microtubules move perpendicular to the field. The microtubules are transported by kinesin motor proteins.

Molecular Sorting by Electrical Steering of Microtubules in Kinesin-Coated Channels

Martin G. L. van den Heuvel, Martijn P. de Graaff, Cees Dekker*

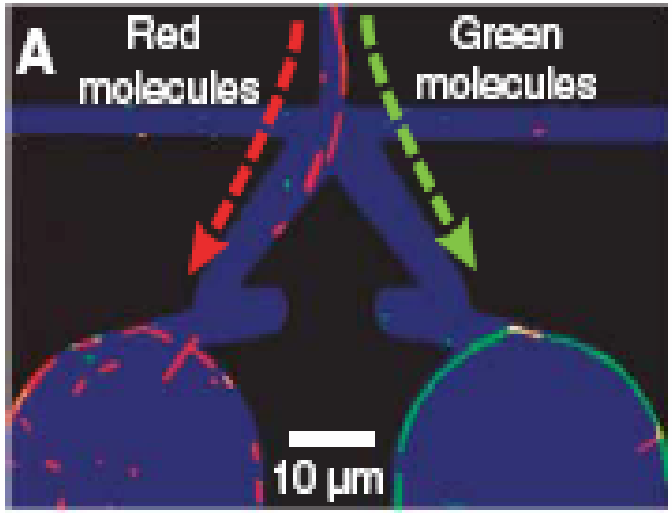

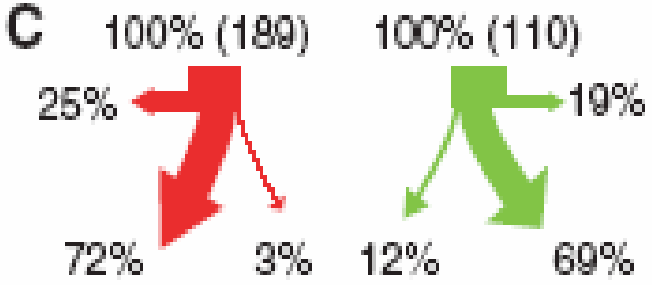

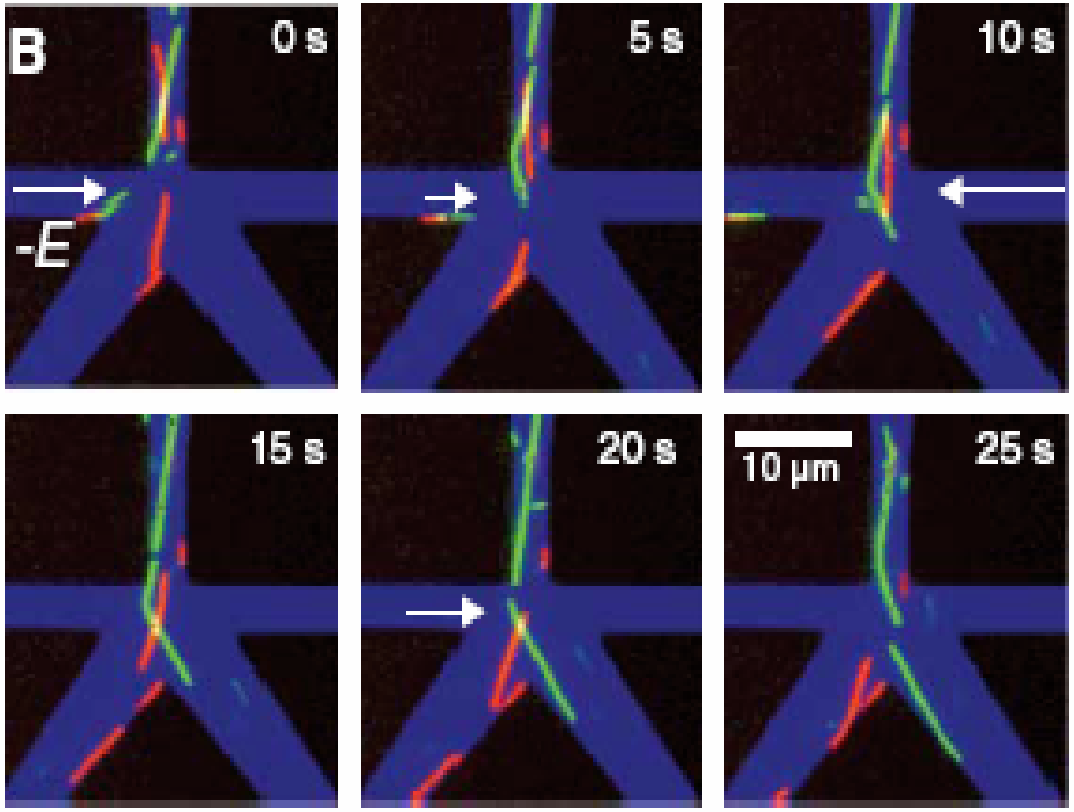

Bacterial flagella: a rotatory motor

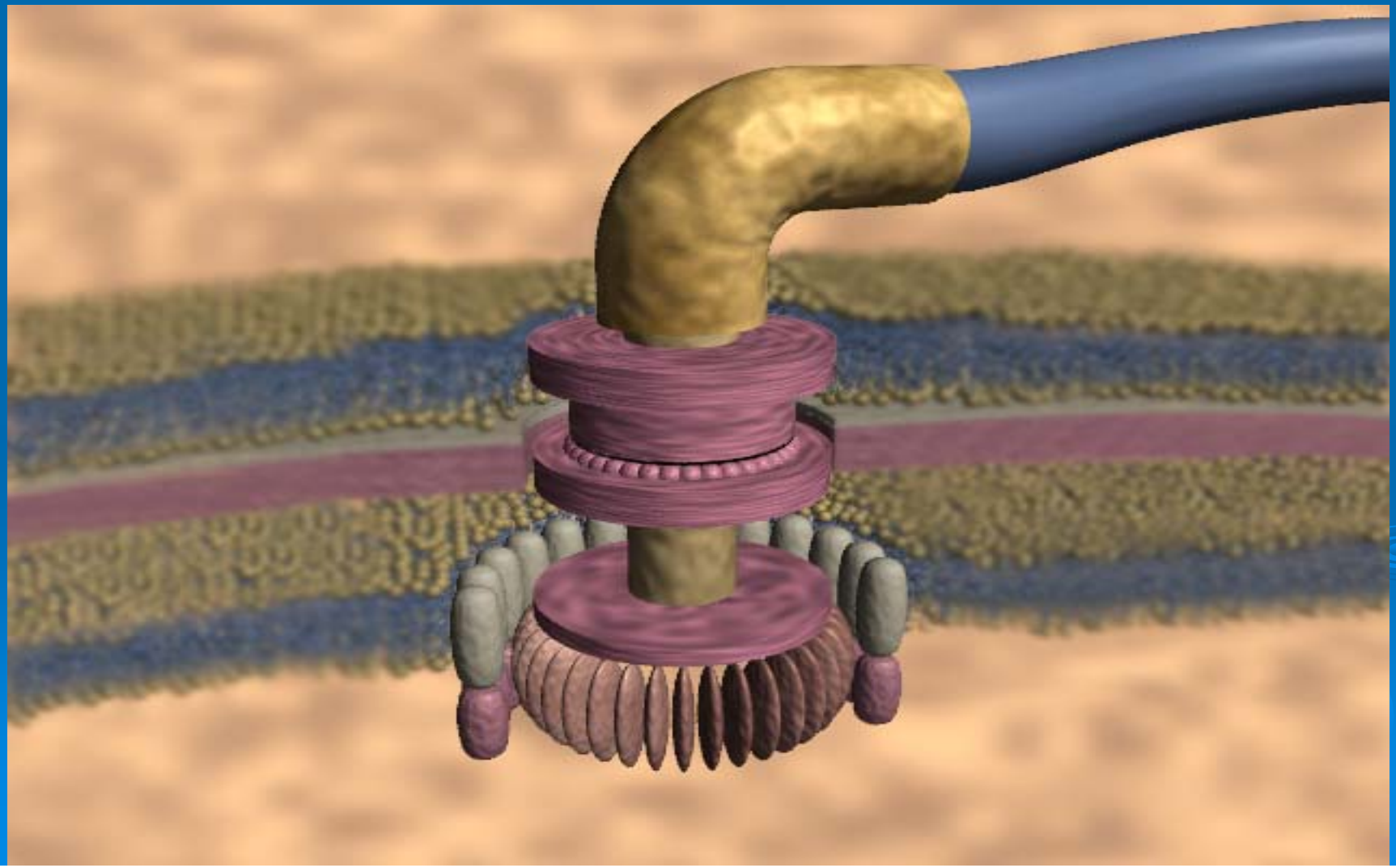

The ATP synthase

The Eukaryotic cell

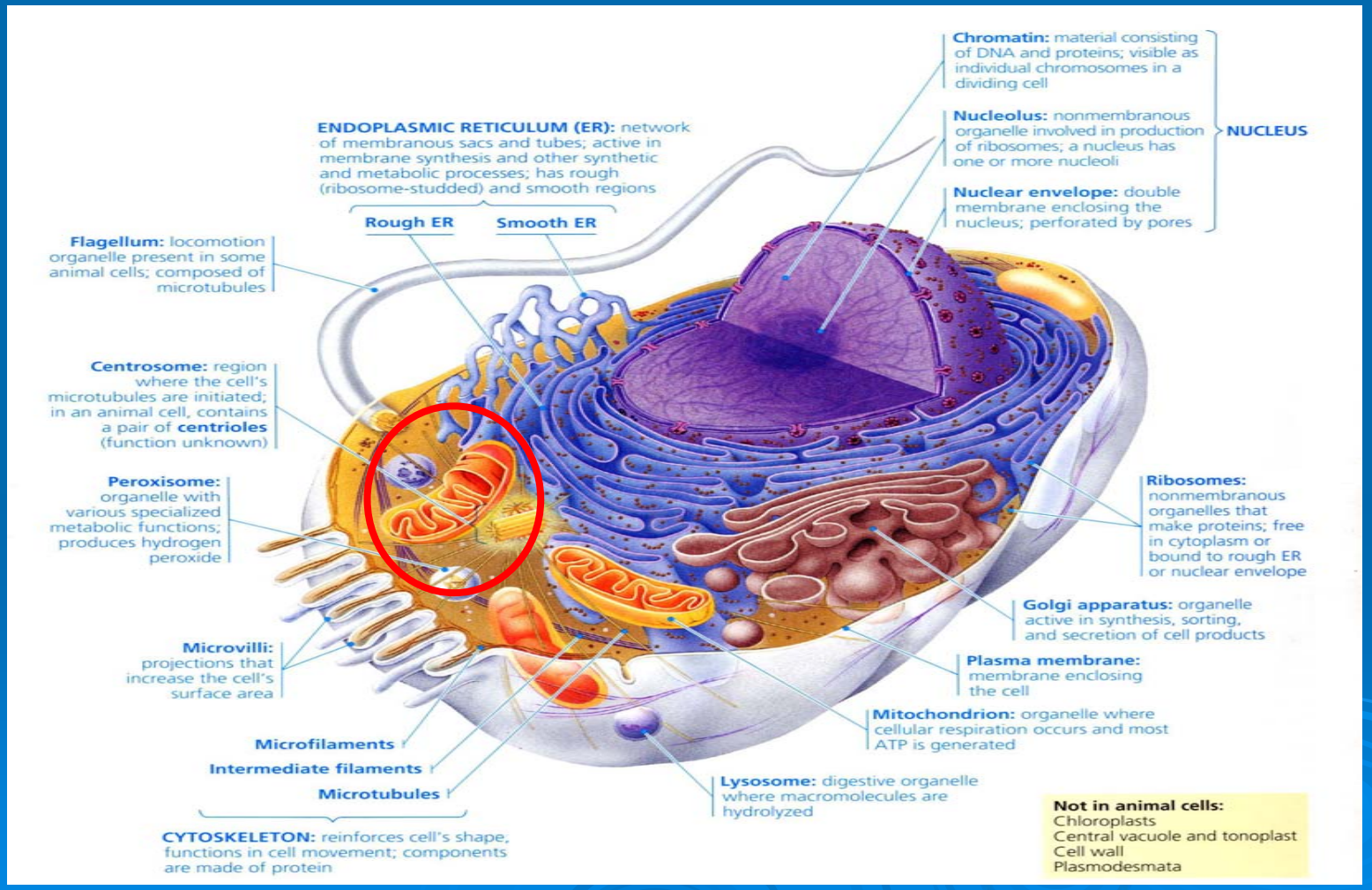

FIGURE 7.7 Overview of an animal cell.

(Campbell Biology, 6th edition)

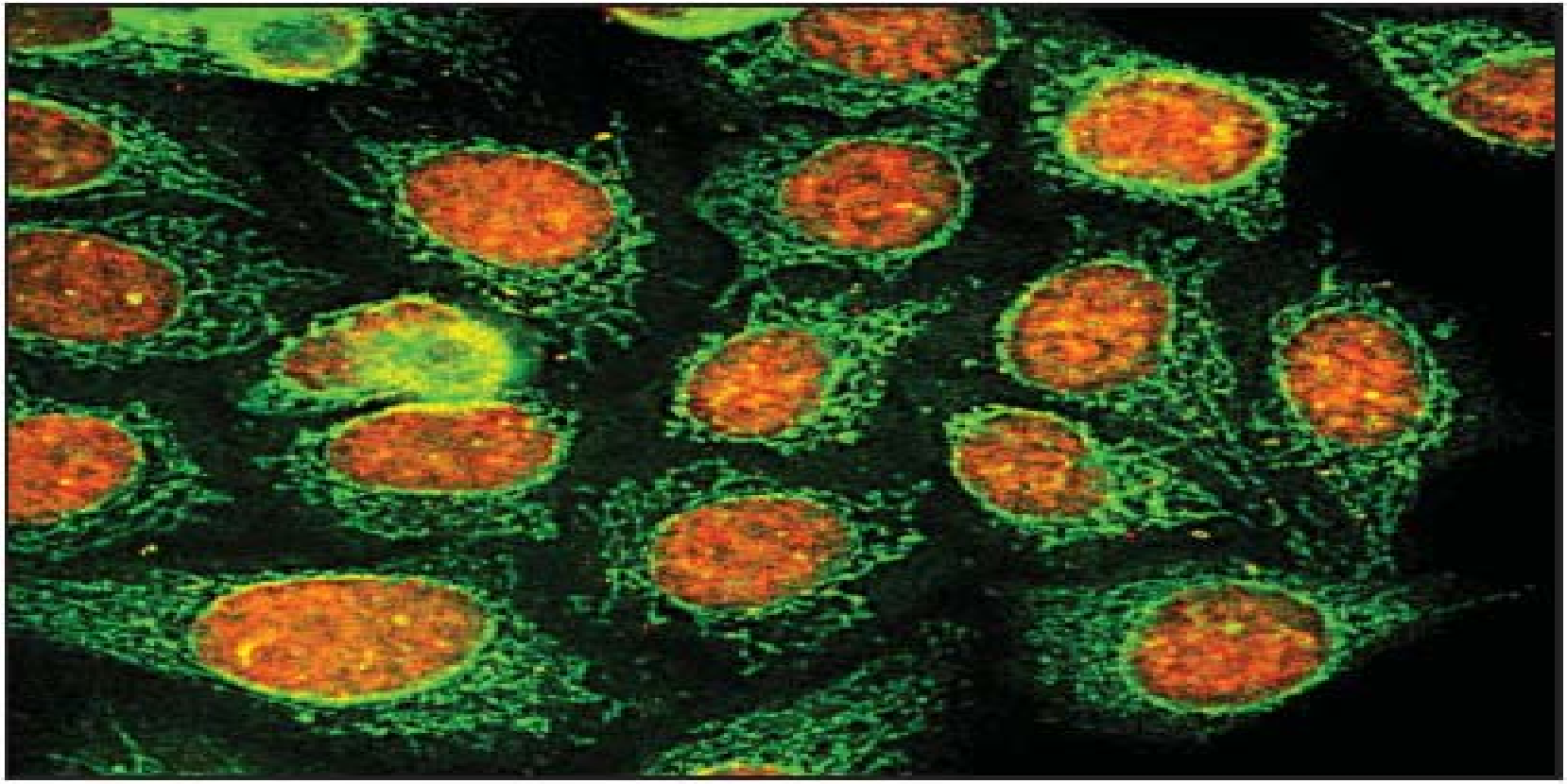

Double duty. Green quantum dots cling to mitochondria in the cytoplasm; orange ones label proteins in the same cells' nuclei.

F_1 and F_0 Proteins in Mitochondria

- Early studies were done with submitochondrial particles (SMP, inside-out vesicles)
- They synthesize ATP in the presence of respiratory substrates, or hydrolyze ATP in the absence of substrates
- Both respiration and ATP hydrolysis generate a Δp in the lumen ⇨ ATP synthesis/ hydrolysis is tightly coupled with Δp
- ATP synthase can be visualized under EM in negatively stained SMP (with phosphotungstate)

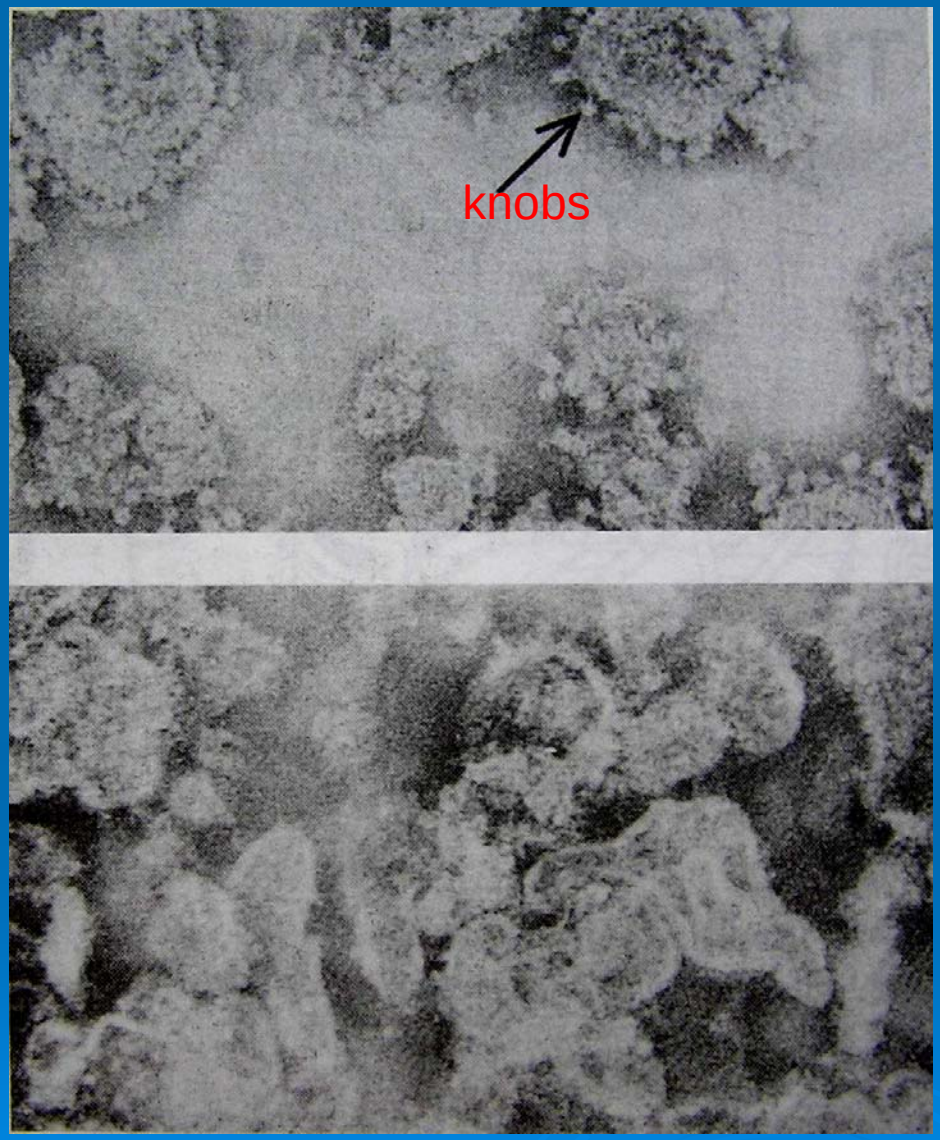

- Negatively stained SMP, with knobs facing outside
- Tightly coupled and sensitive to oligomycin

- Wash with urea/chelating agents, knobs were lost
- SMP became uncoupled, that is inhibited by oligomycin
- The H^+ channel was termed F_0 (fraction oligomycin)

- F_0 – hydrophobic, forming H^+ channel and coupling H^+ to ATP synthesis
- F_1 – hydrophilic, site of ATP synthesis

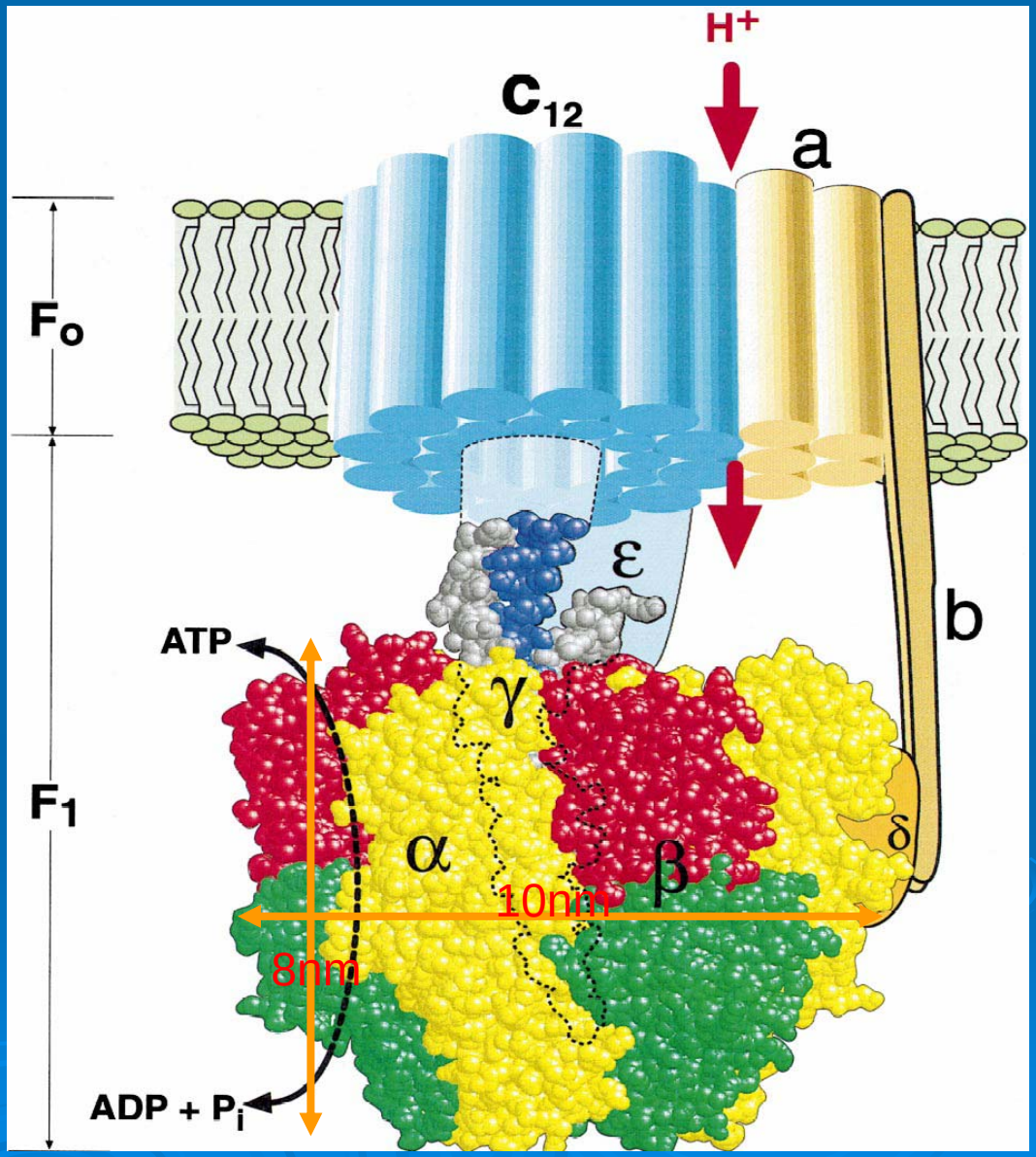

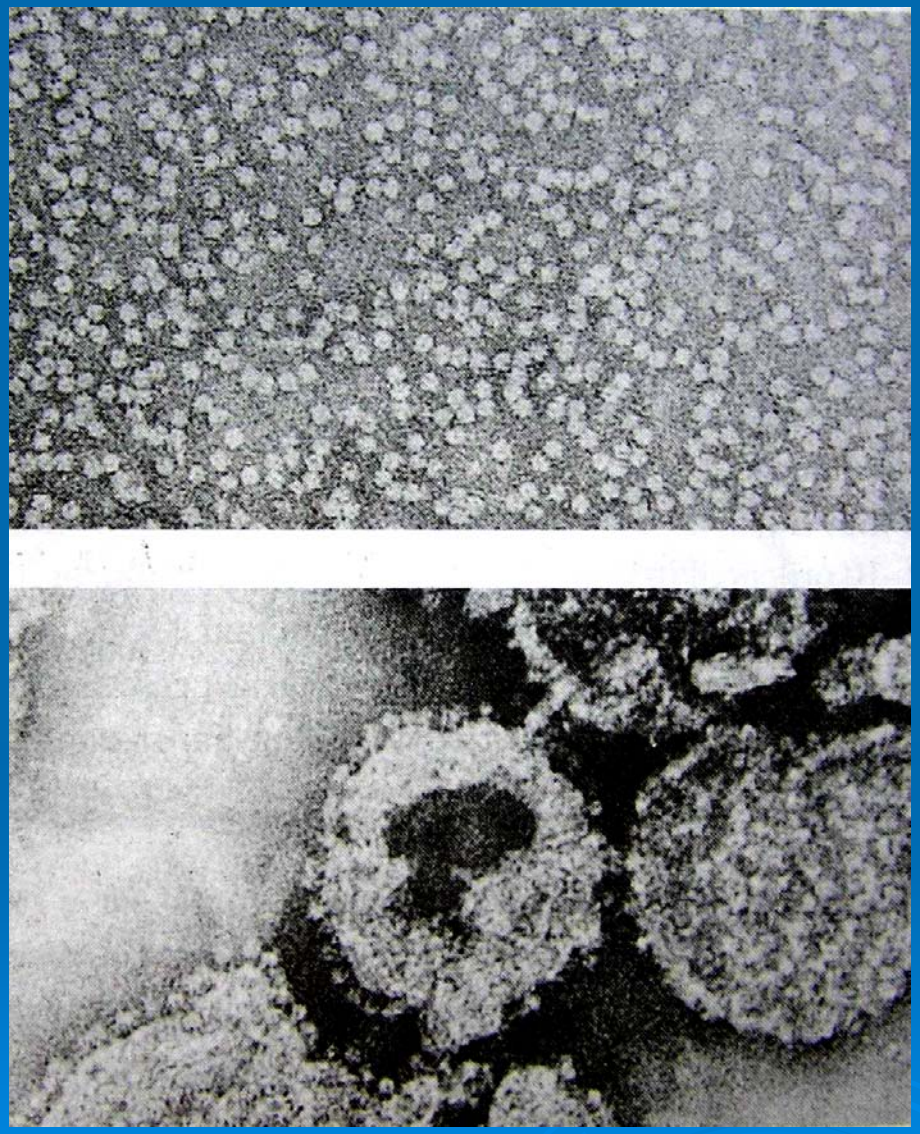

- ATPase activity was isolated, and not inhibited by oligomycin (termed F_1, fraction 1)
- After reconstitution, coupling was back
- F_1 acts as a plug on F_0

The assembly of F0 and F1

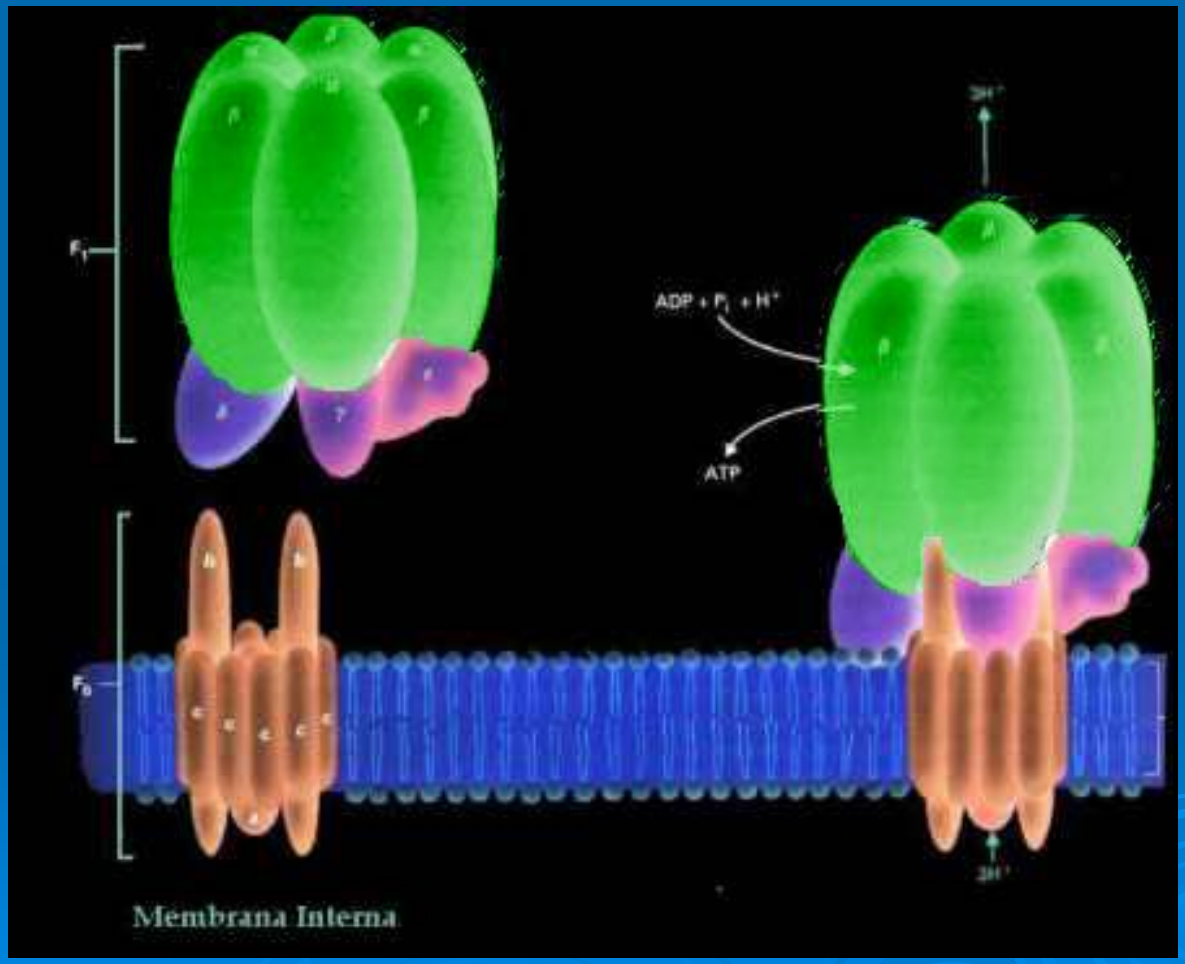

yeast

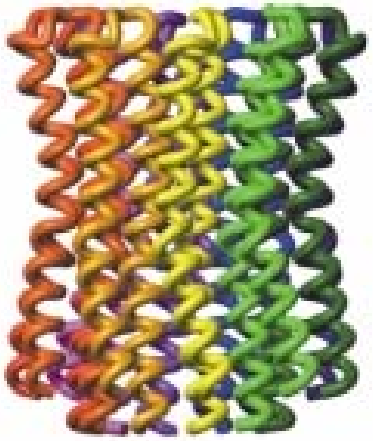

10 copies
in yeast

spinach

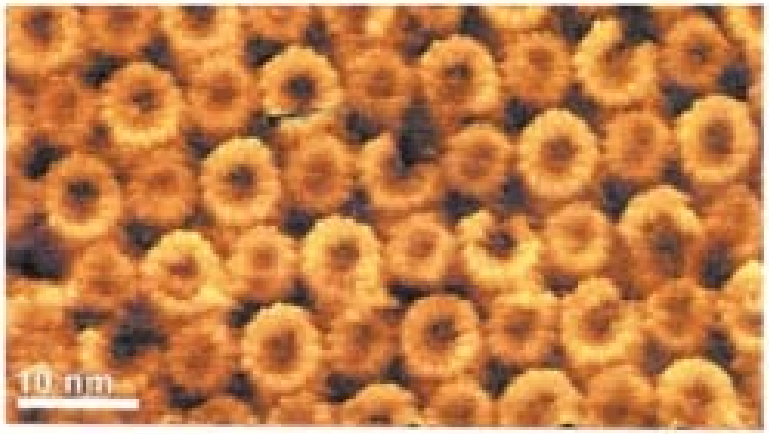

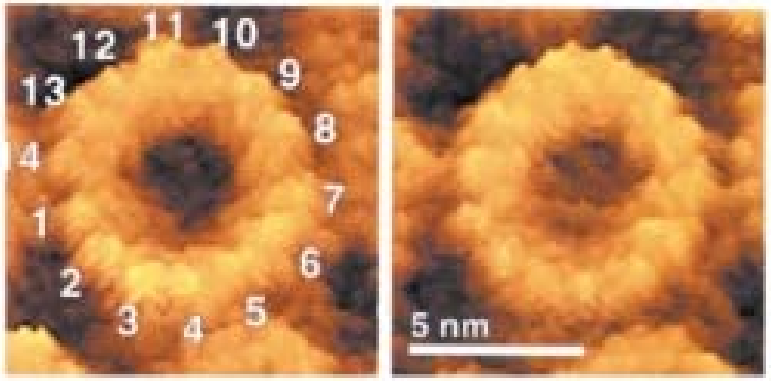

14 copies
in spinach
chloroplasts

Ilyobacter

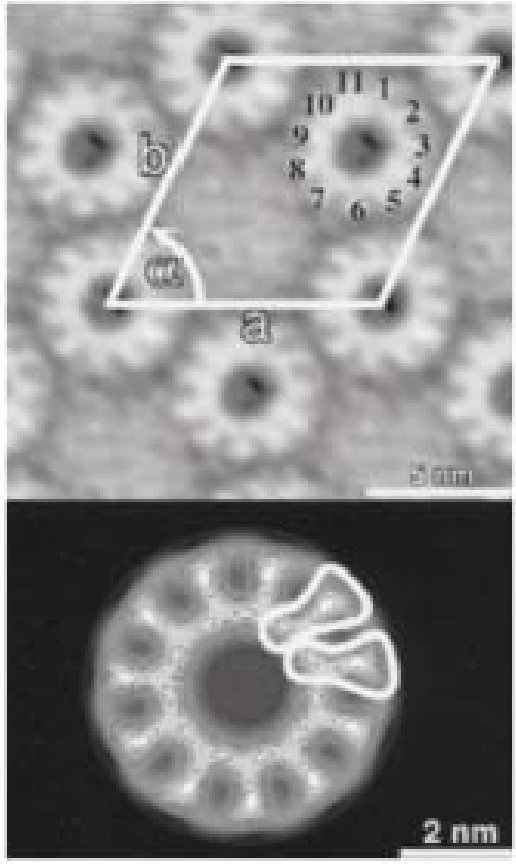

11 copies
in *Ilyobacter*

- The F_0 motor is made up of a transmembrane cylinder of 10–14 c subunits, depending on the species

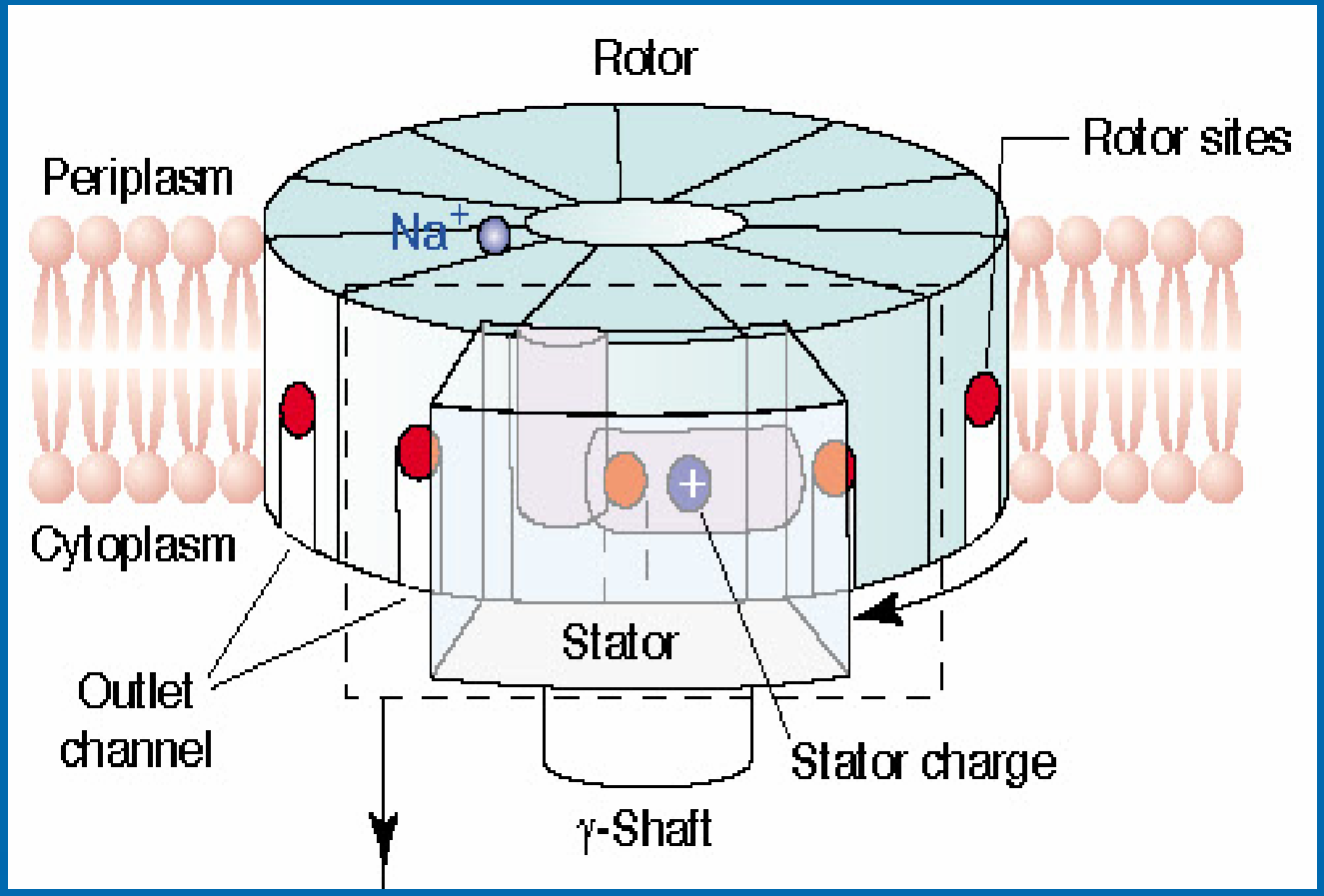

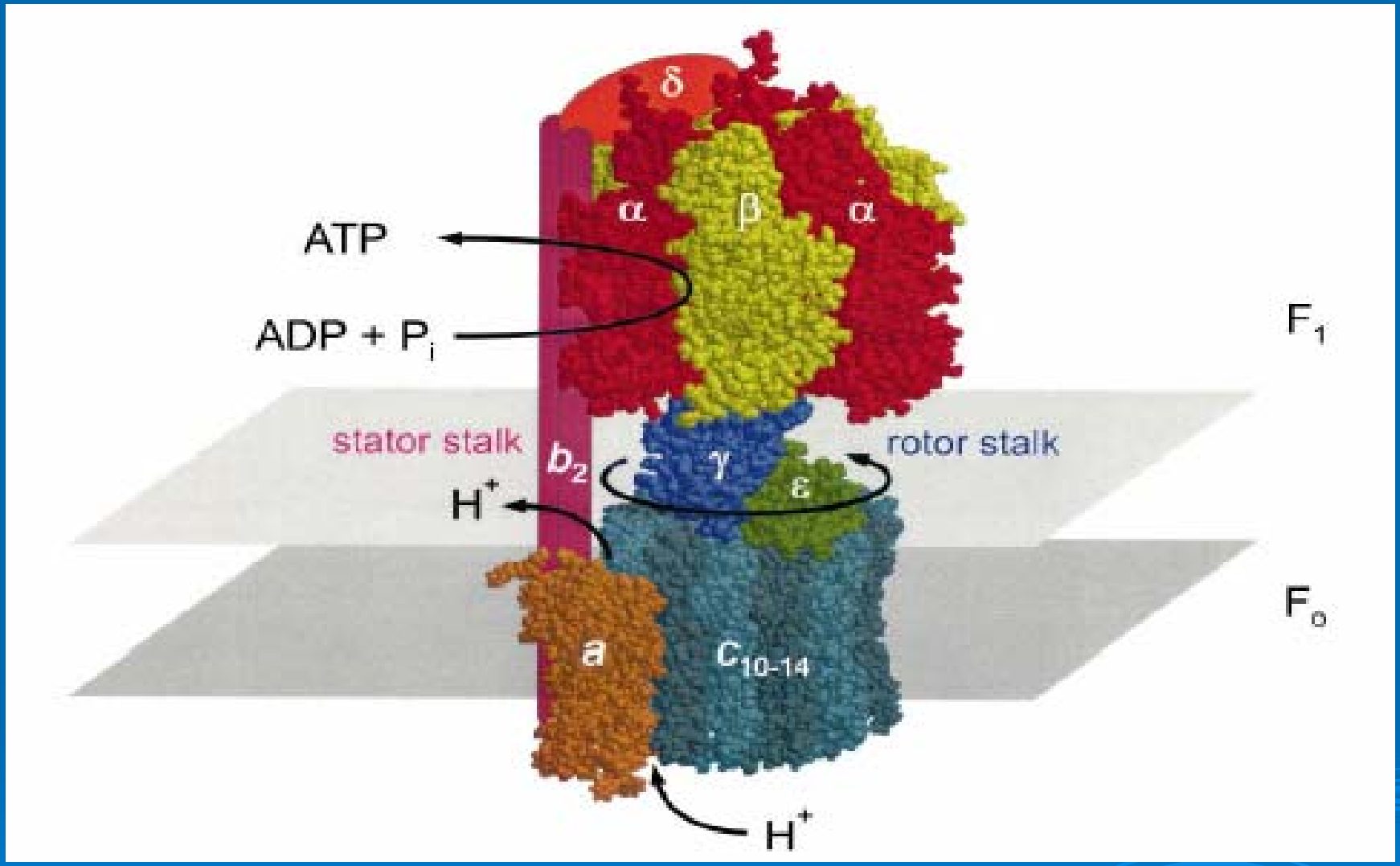

E.Coli ATP synthase

c, γ and ε are rotor, a, b, α, β and δ are stator

Visualize the rotation

- A $\alpha_3\beta_3\gamma$ complex from bacteria
- N terminus of β had polyhistidine tag attached, which enabled the anchoring of the complex to microscopic slide coated with Ni ions
- All the naturally occurring cysteine residues were removed, and insert one in γ at a position distant from the $\alpha\beta$ core
- A long and fluorescent labeled actin filament was attached to the single introduced cystein

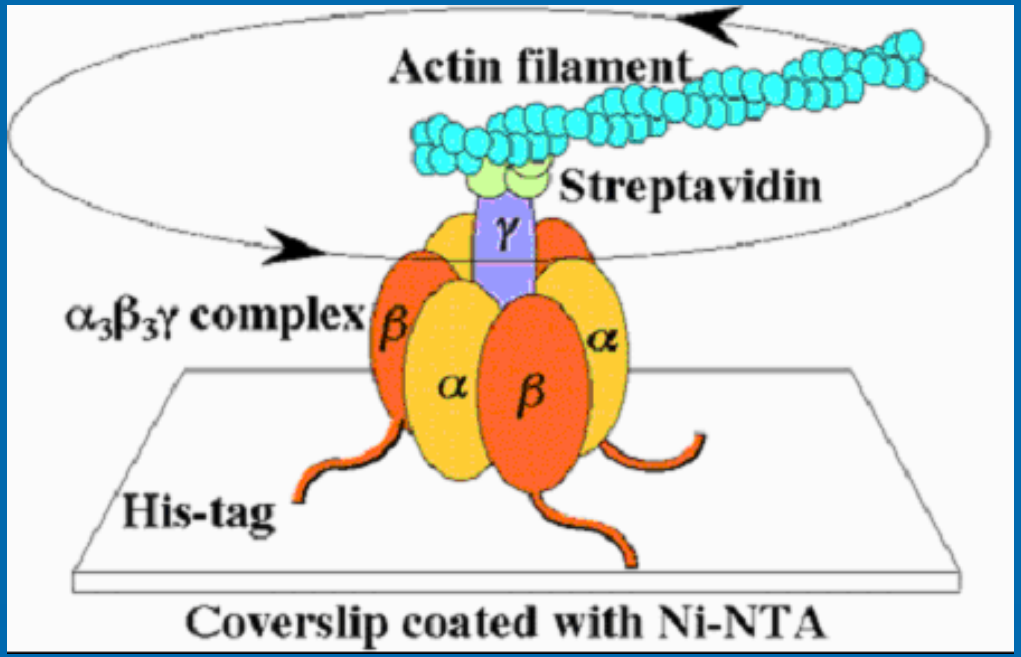

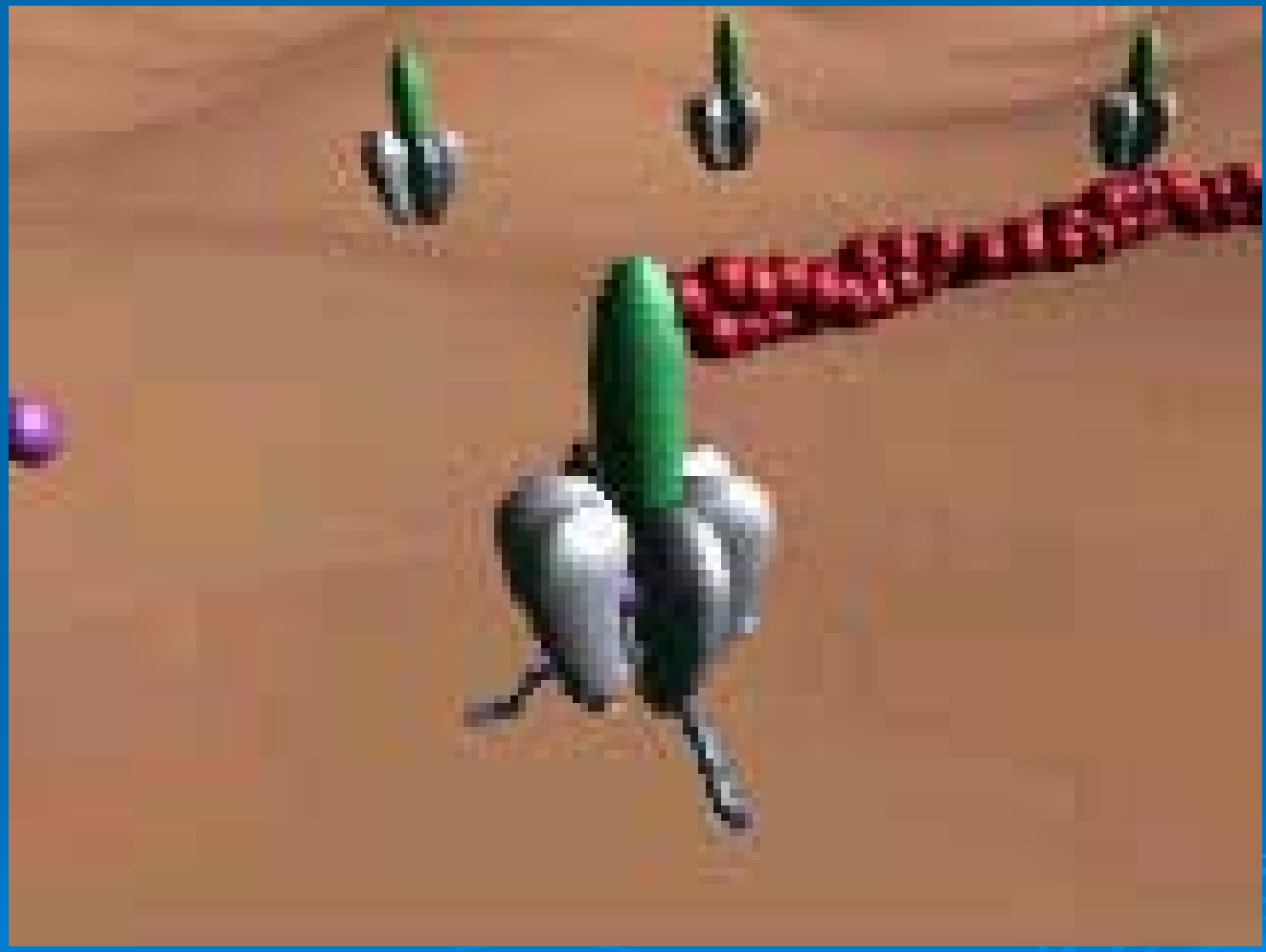

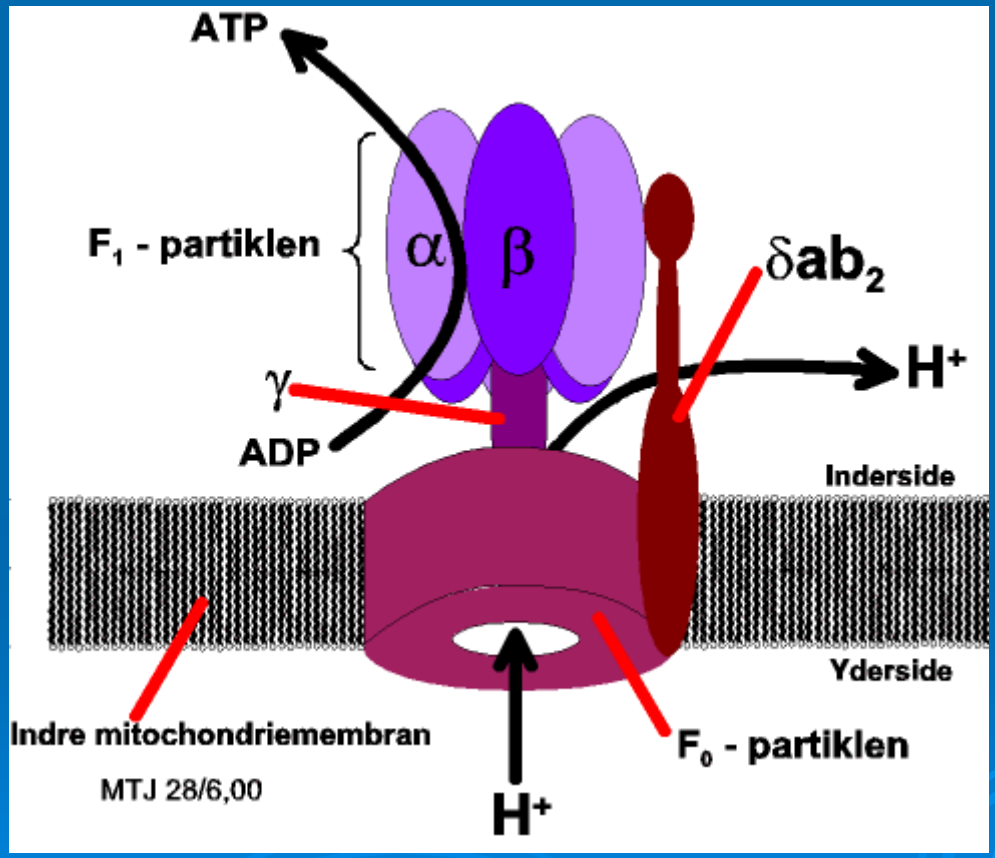
ATP
F1 - partiklen
α
β
δab2
H+
γ
ADP
Inderside
Yderside
Indre mitochondriemembran
MTJ 28/6,00
H+
F0 - partiklen

How to prepare your nano-materials?

1. Protein molecules by genetic engineering
2. Nano propeller by nanofibricated technology

How to assemble these materials?

Recombinant protein production

Genetic engineering

基因工程(Genetic Engineering)

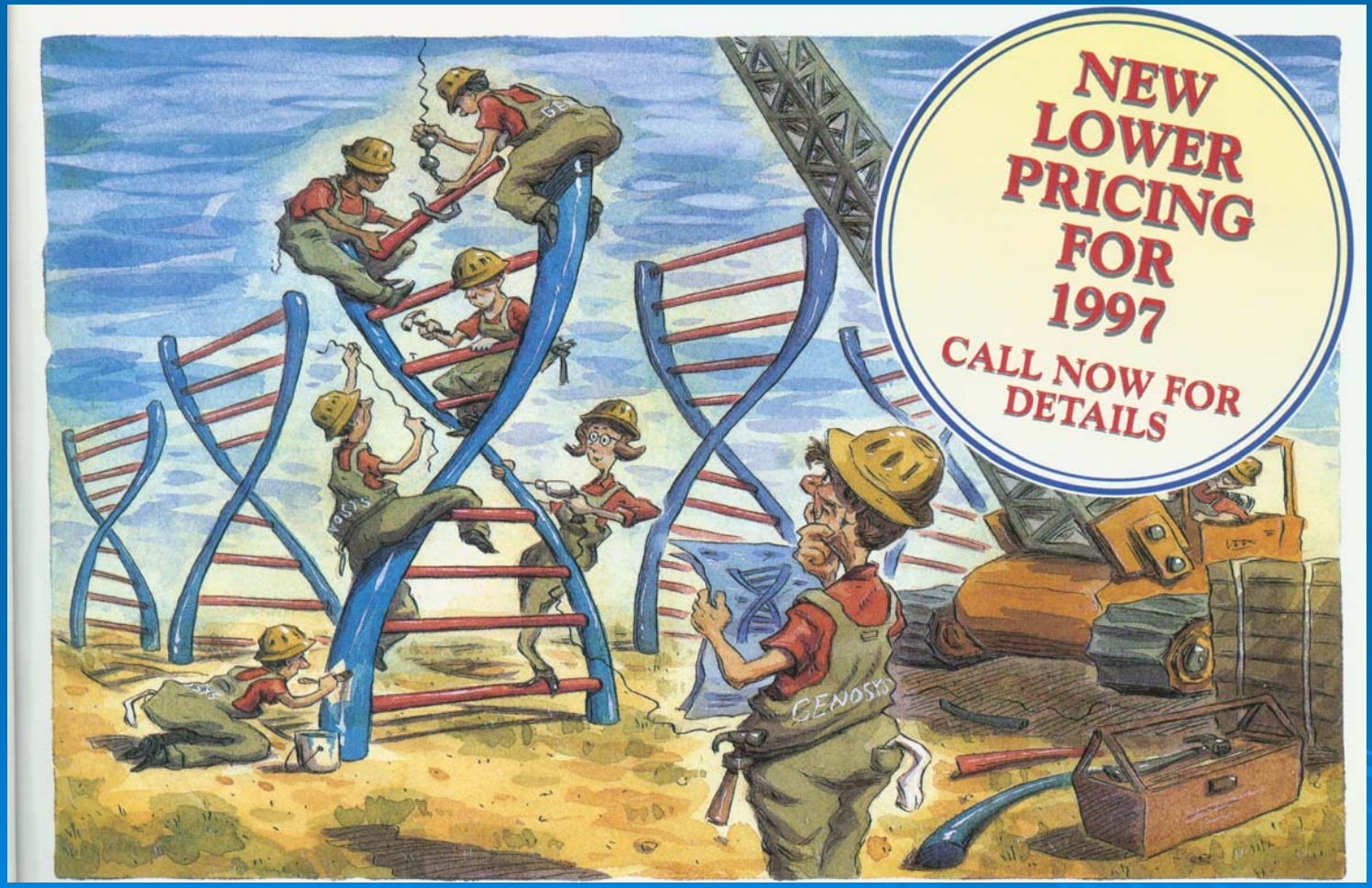


Zucchana
60¢
per base

The Obesity Gene

The mouse on the left has a defective gene that causes obesity. Researchers have found a human relative of this gene.

Trimming down. Mice that can't respond to the appetite-regulating hormone leptin grow obese (*right*). Mice lacking the perilipin protein that coats lipid droplets burn off the excess fat and become almost as slender (*middle*) as normal mice (*left*).

Science, VOL.311, 2006, P. 1232-1234

比利時藍牛 (Belgian blue)

Mutation in Myostadin

Natural boost. A Berlin child who carries a mutation in the myostatin gene has had bodybuilder muscles since birth.

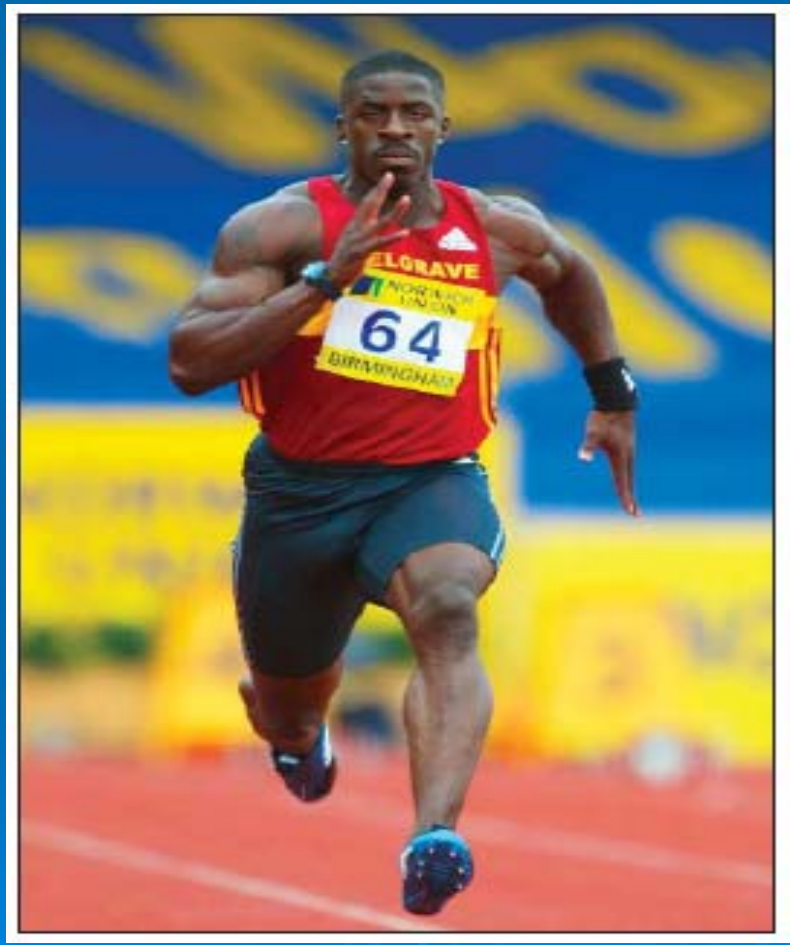

Schrödinger
LIFE AND THOUGHT

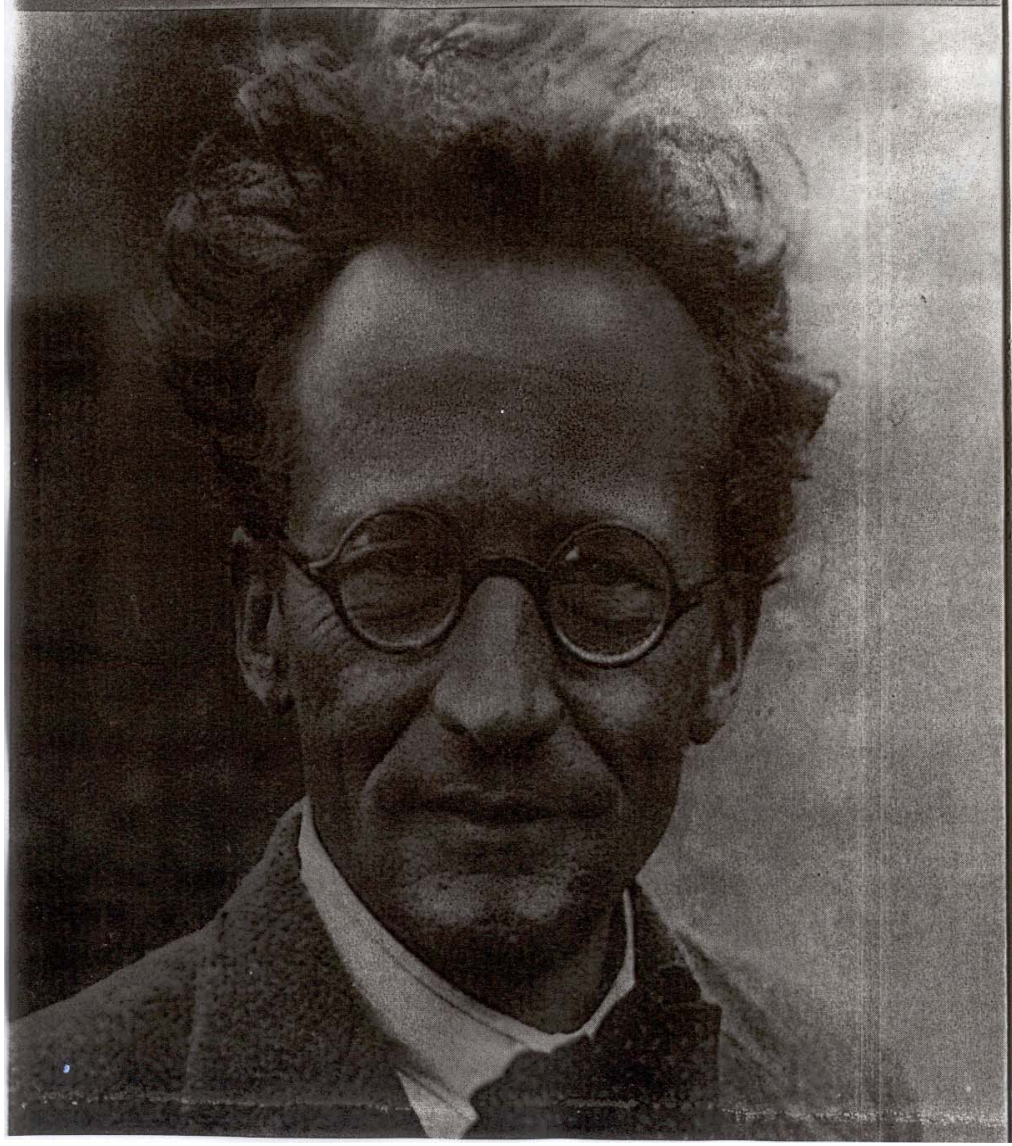

WHAT IS LIFE?

with Mind and Matter *and*
Autobiographical Sketches

ERWIN SCHRÖDINGER

canto

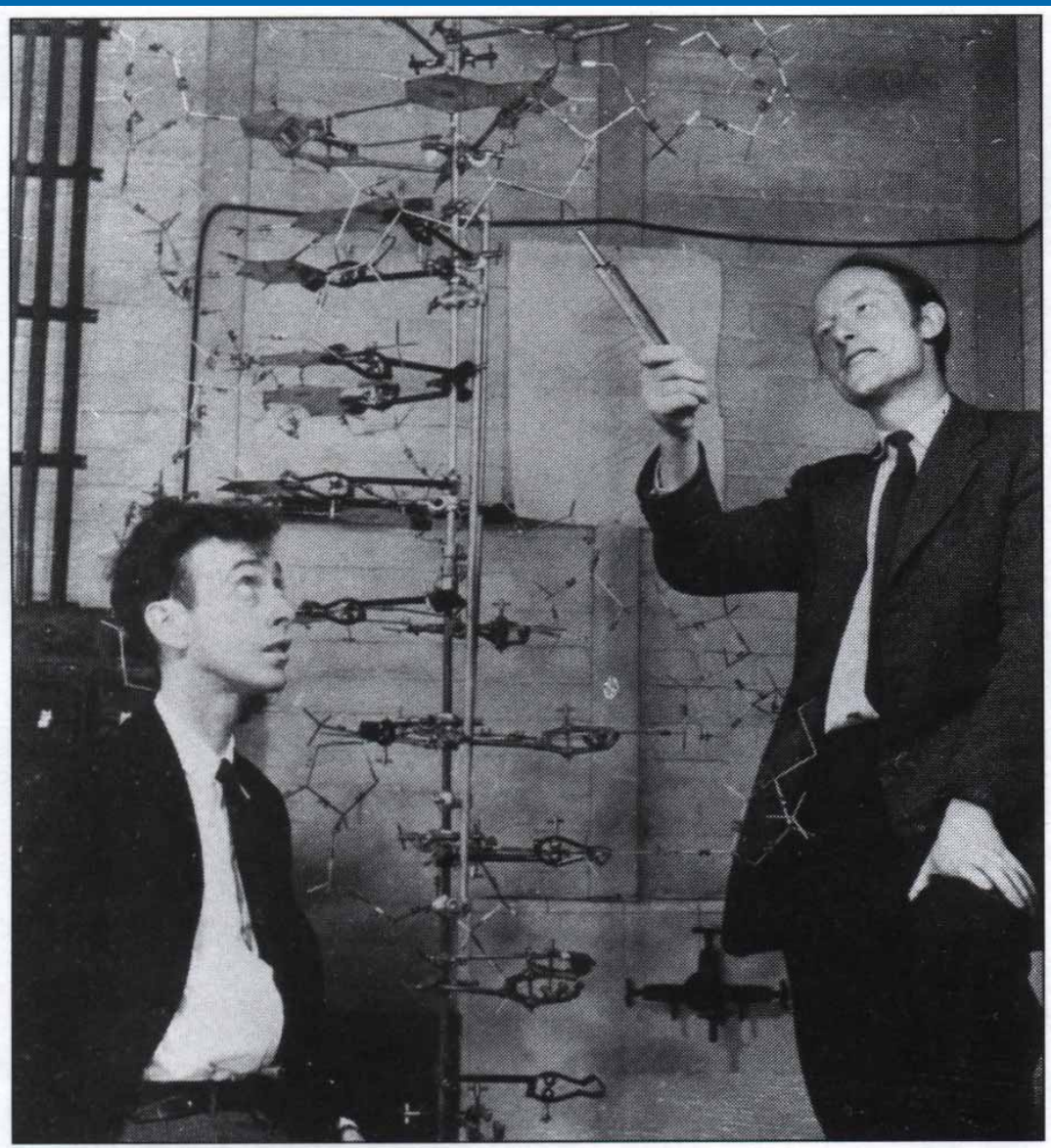

Figure 1.9 James Watson (left) and Francis Crick.

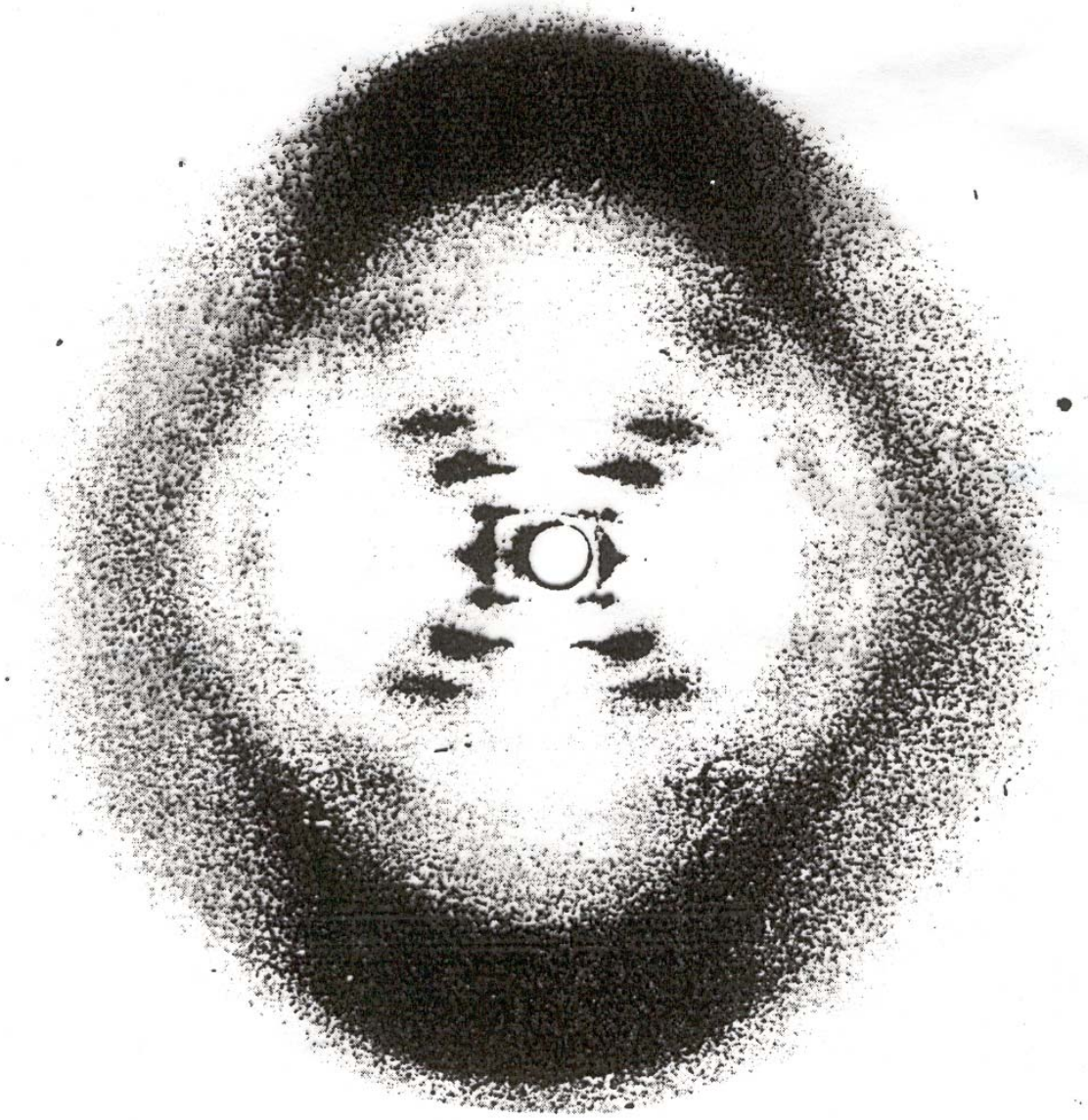

An X-ray photograph of DNA in the B form, taken by Rosalind Franklin late in 1952.

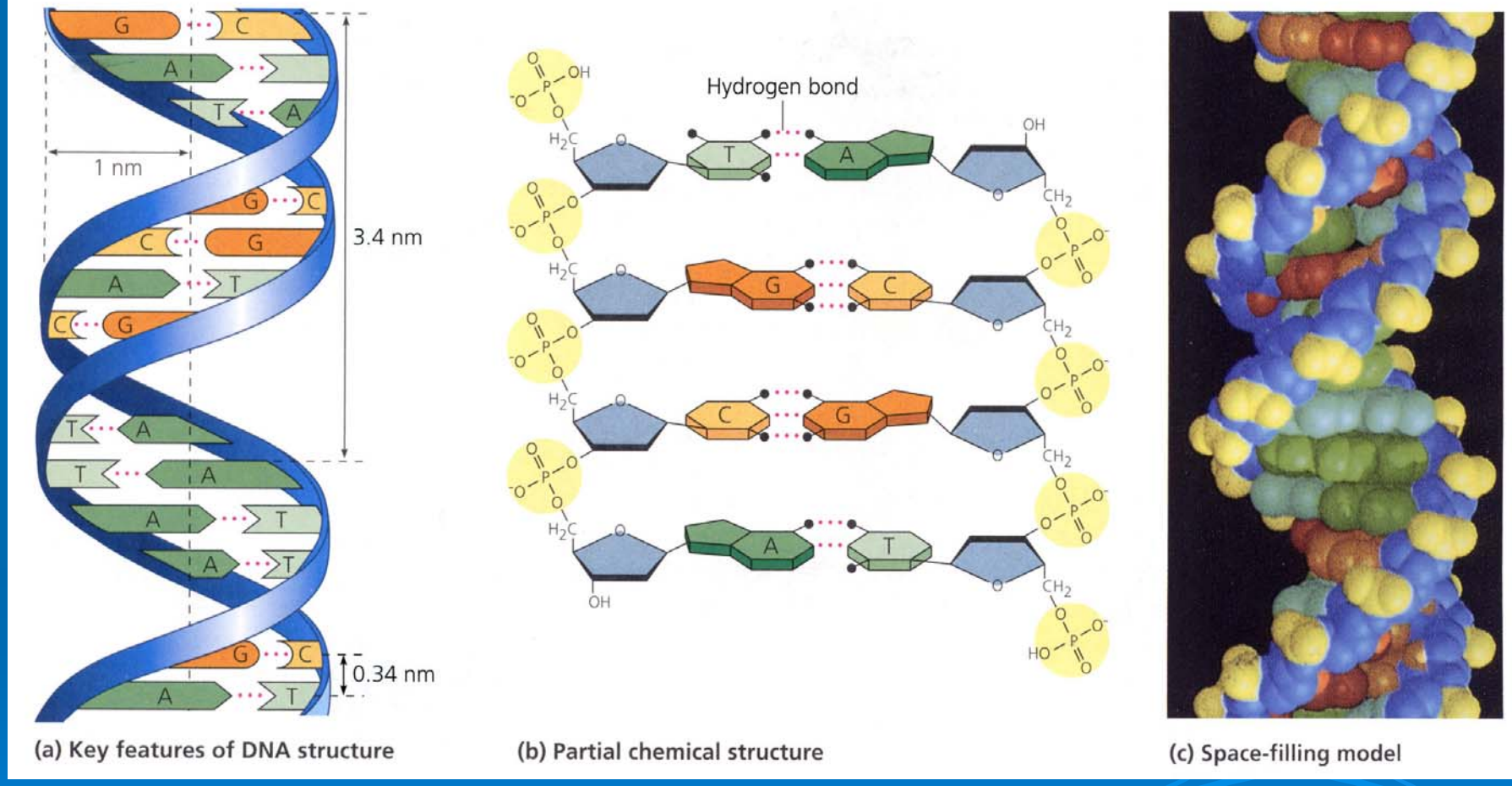

FIGURE 16.5 The double helix.

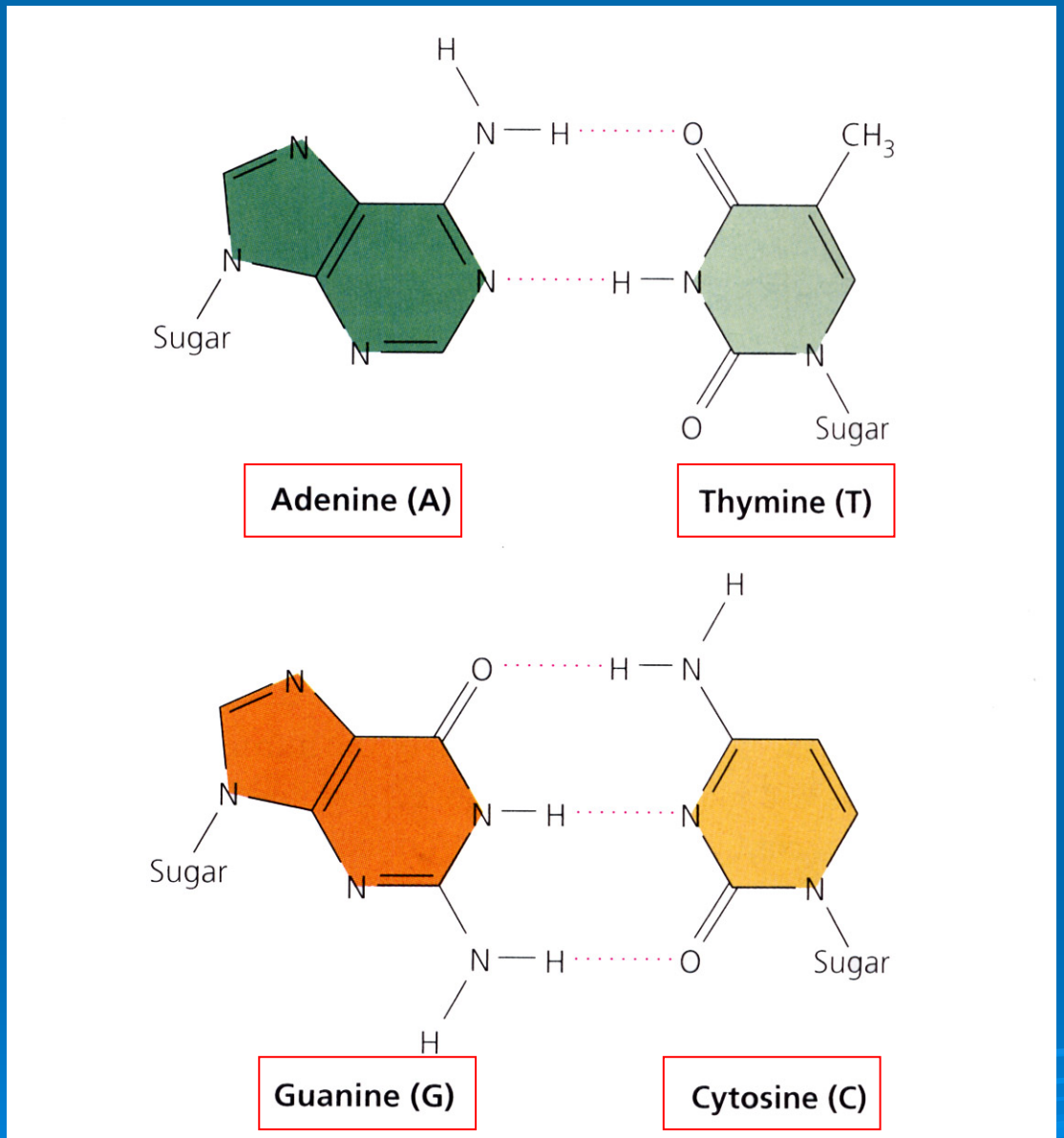

FIGURE 16.6 Base pairing in DNA.

基因: 染色體上的雙股DNA的排列順序

字母

.....ATGCCGTA.....

.....TACGGCAT.....

BED

BAD

BAT

單字

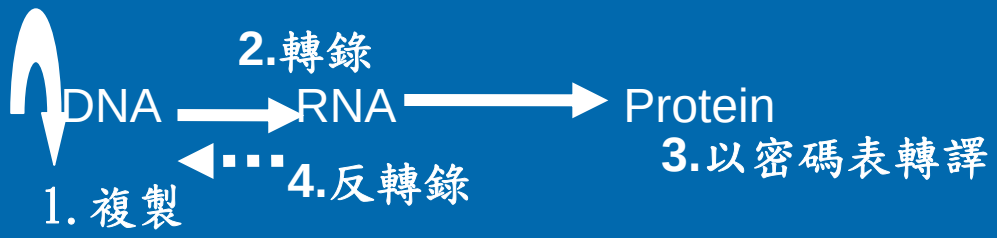

First base (5′ end)	Second base: U	Second base: C	Second base: A	Second base: G	Third base (3′ end)
U	UUU Phe	UCU Ser	UAU Tyr	UGU Cys	U
	UUC Phe	UCC Ser	UAC Tyr	UGC Cys	C
	UUA Leu	UCA Ser	UAA Stop	UGA Stop	A
	UUG Leu	UCG Ser	UAG Stop	UGG Trp	G
C	CUU Leu	CCU Pro	CAU His	CGU Arg	U
	CUC Leu	CCC Pro	CAC His	CGC Arg	C
	CUA Leu	CCA Pro	CAA Gln	CGA Arg	A
	CUG Leu	CCG Pro	CAG Gln	CGG Arg	G
A	AUU Ile	ACU Thr	AAU Asn	AGU Ser	U
	AUC Ile	ACC Thr	AAC Asn	AGC Ser	C
	AUA Ile	ACA Thr	AAA Lys	AGA Arg	A
	AUG Met or start	ACG Thr	AAG Lys	AGG Arg	G
G	GUU Val	GCU Ala	GAU Asp	GGU Gly	U
	GUC Val	GCC Ala	GAC Asp	GGC Gly	C
	GUA Val	GCA Ala	GAA Glu	GGA Gly	A
	GUG Val	GCG Ala	GAG Glu	GGG Gly	G

圖二 生命科學中定理與密碼表

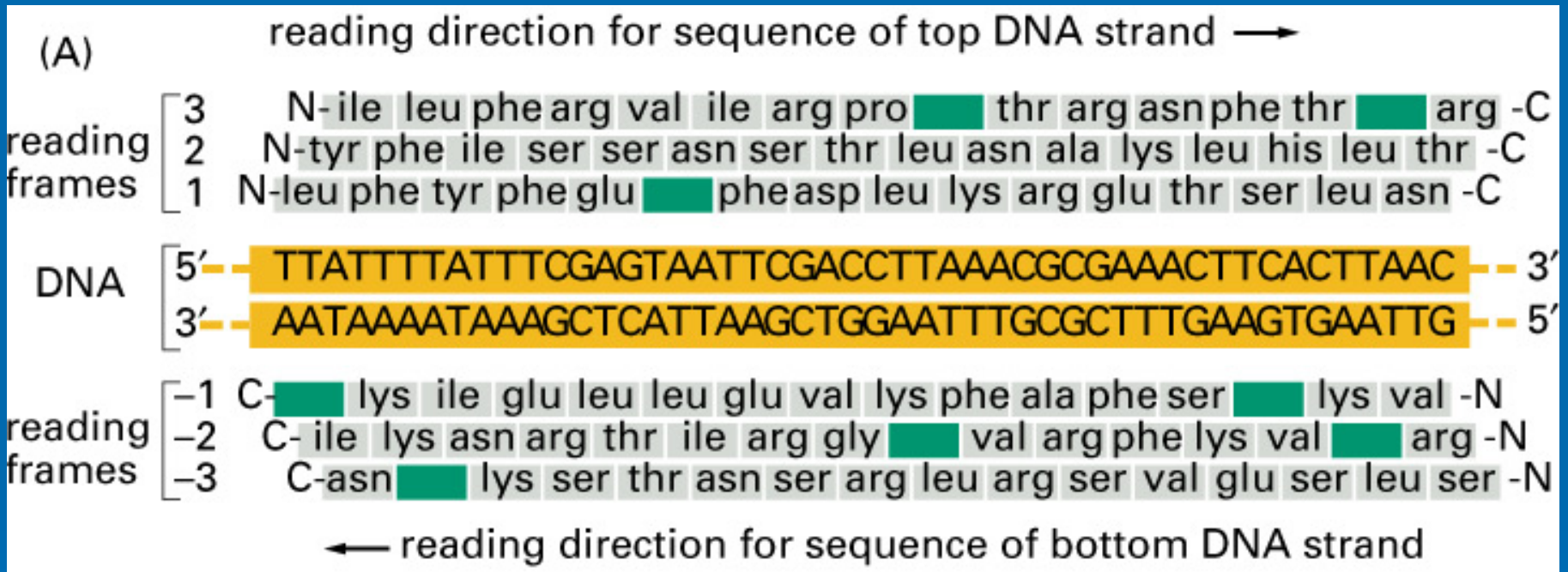

Figure 8–38 part 1 of 2. Molecular Biology of the Cell, 4th Edition.

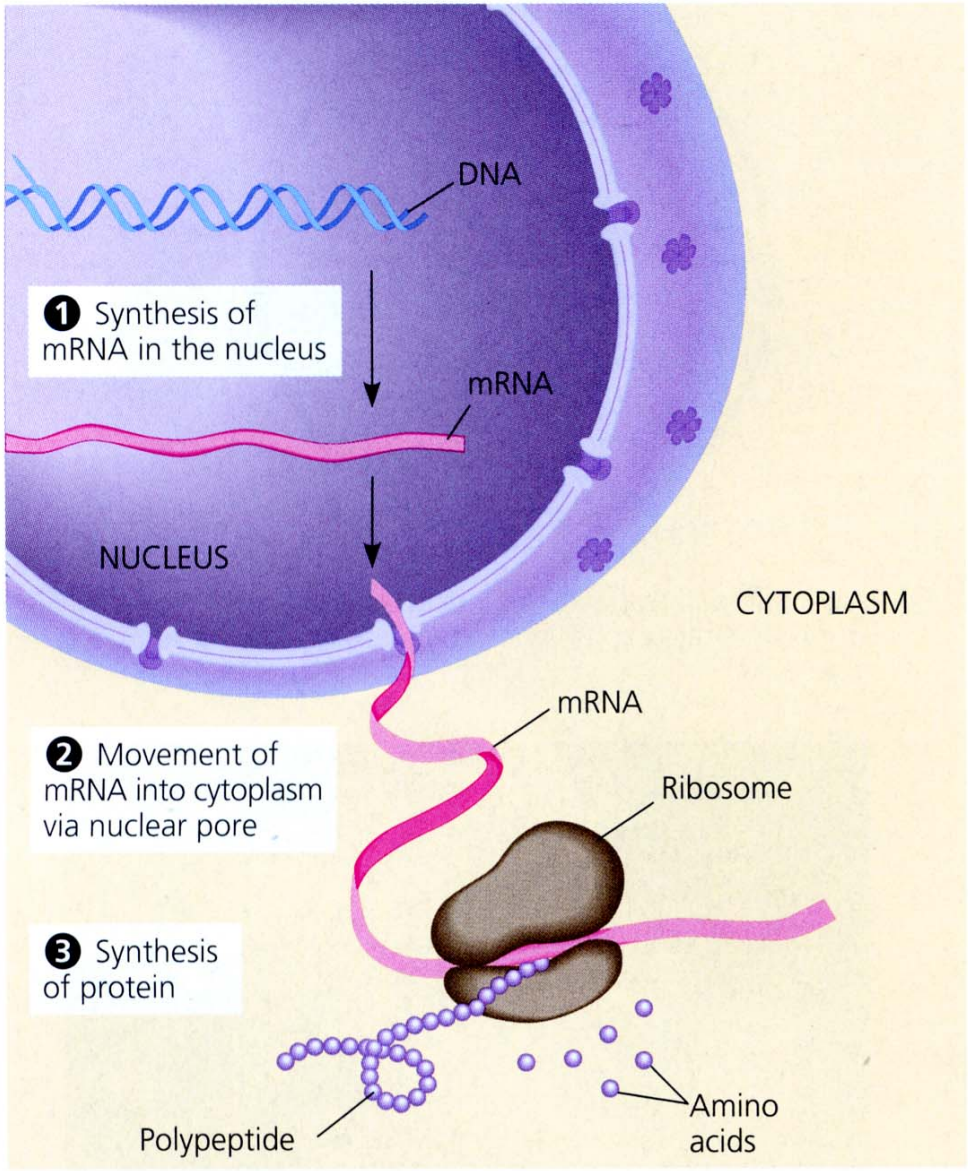

FIGURE 5.28 DNA ⟶ RNA ⟶ protein: a diagrammatic overview of information flow in a cell.

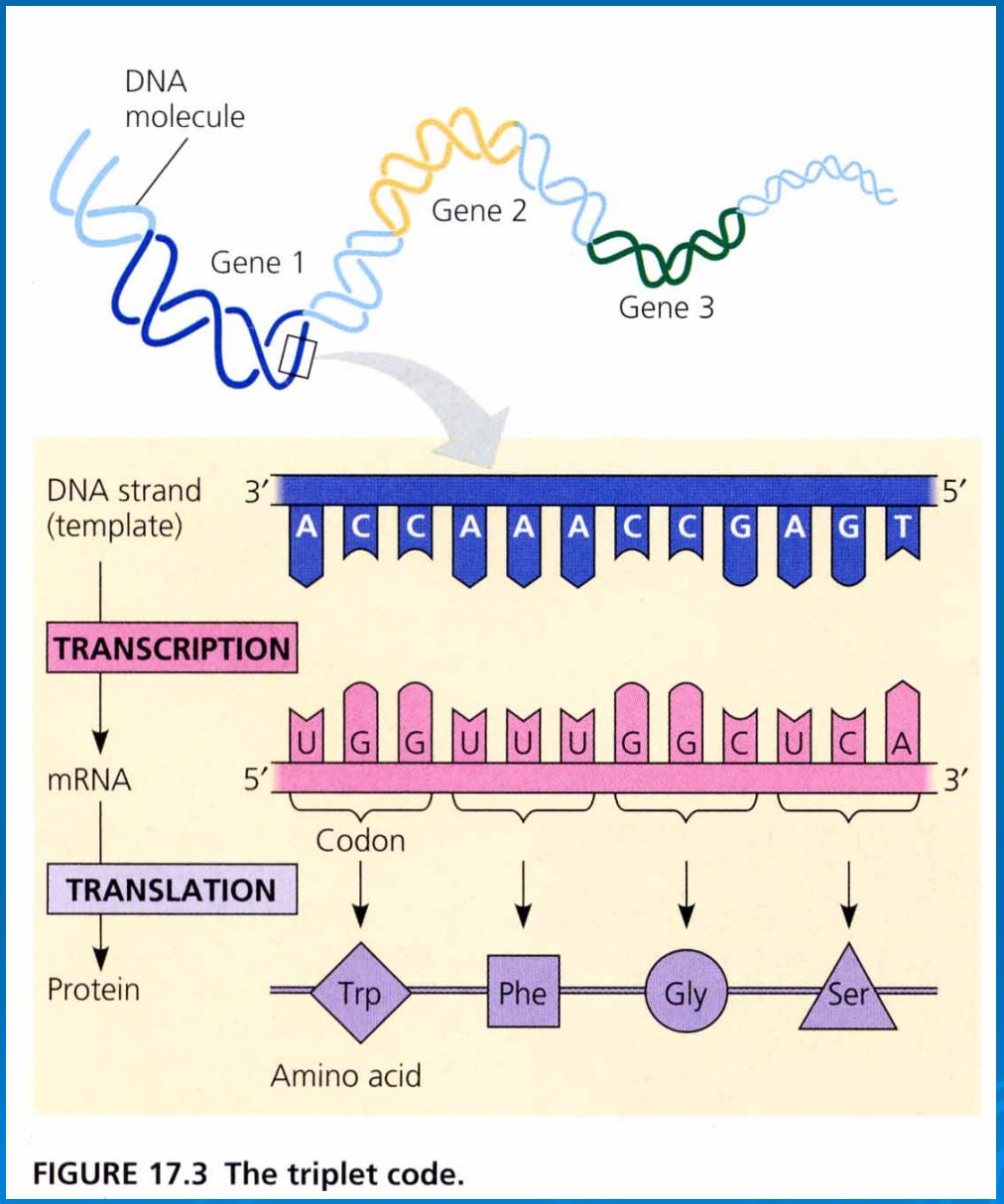

FIGURE 17.3 The triplet code.

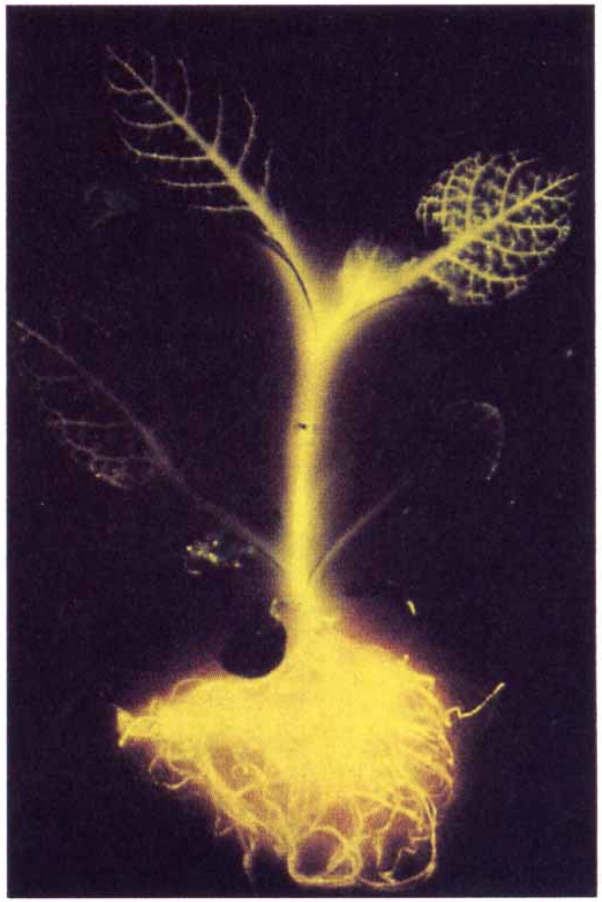

FIGURE 17.5 A tobacco plant expressing a firefly gene.


1ml IRES
6'th days

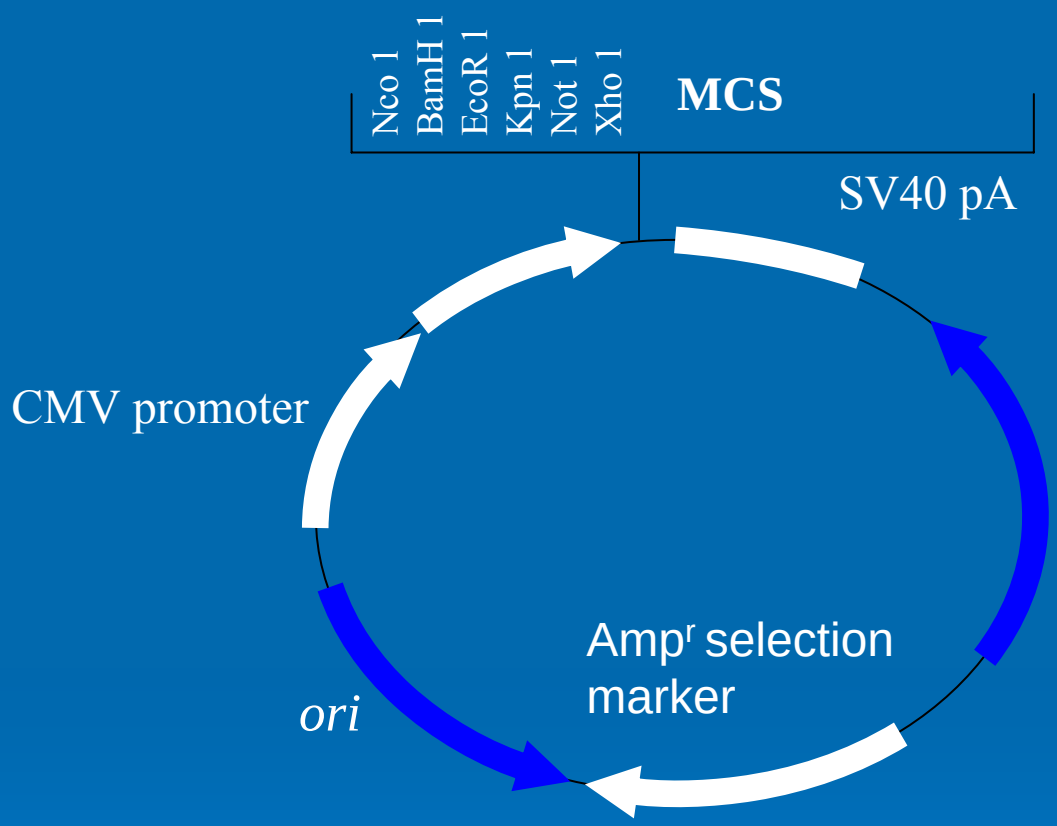

圖三:表現載體 (expression vector)

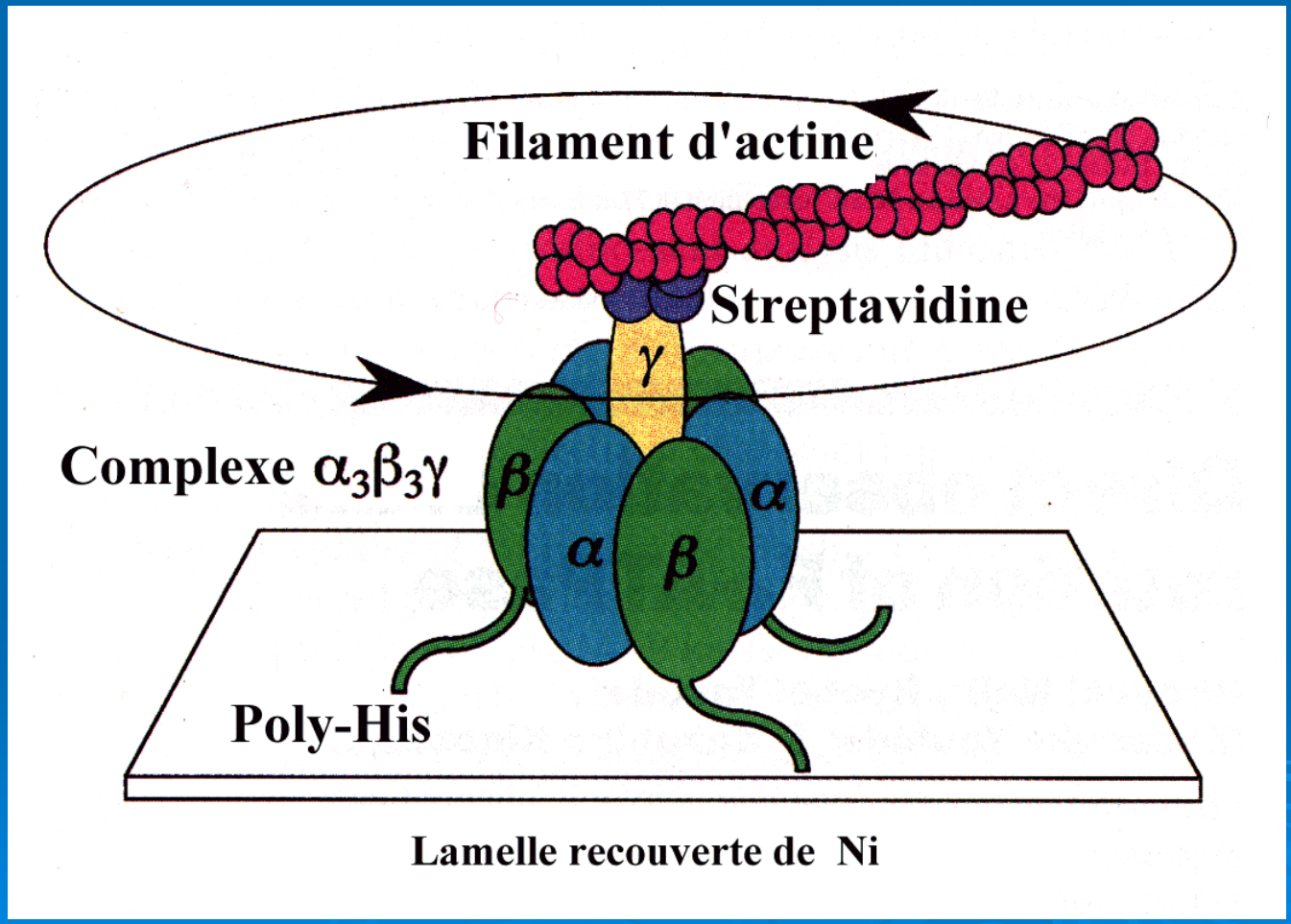
Filament d'actine
Streptavidine
γ
Complexe $\alpha_3\beta_3\gamma$
β
α
α
β
Poly-His
Lamelle recouverte de Ni

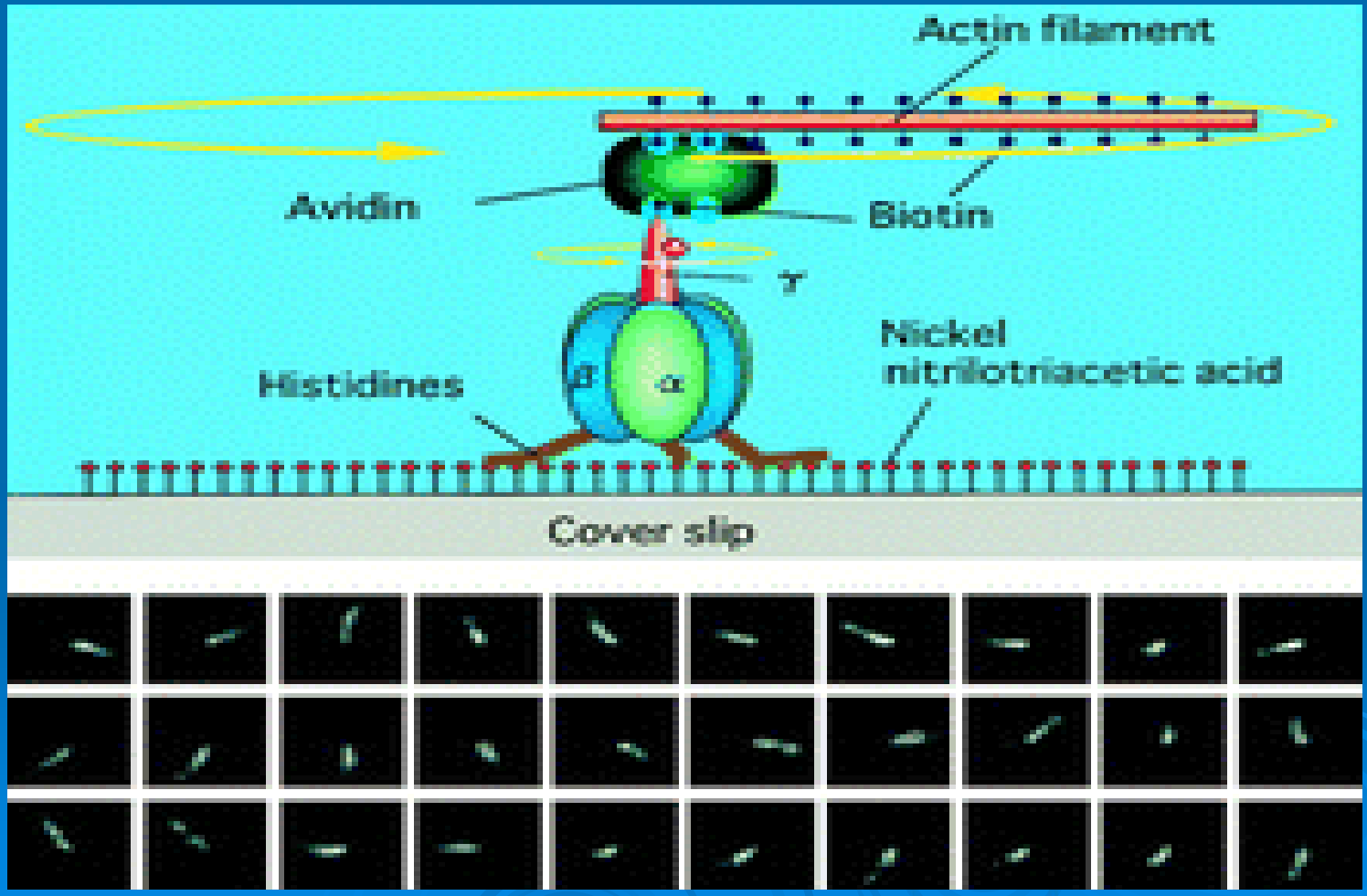
Actin filament
Avidin
Biotin
γ
Nickel
nitrilotriacetic acid
Histidines
β
α
Cover slip

Powering an Inorganic Nanodevice with a Biomolecular Motor

Ricky K. Soong,[1,2] George D. Bachand,[1,2] Hercules P. Neves,[1,2] Anatoli G. Olkhovets,[1,3] Harold G. Craighead,[1,3] Carlo D. Montemagno[1,2]*

Biomolecular motors such as F_1–adenosine triphosphate synthase (F_1-ATPase) and myosin are similar in size, and they generate forces compatible with currently producible nanoengineered structures. We have engineered individual biomolecular motors and nanoscale inorganic systems, and we describe their integration in a hybrid nanomechanical device powered by a biomolecular motor. The device consisted of three components: an engineered substrate, an F_1-ATPase biomolecular motor, and fabricated nanopropellers. Rotation of the nanopropeller was initiated with 2 mM adenosine triphosphate and inhibited by sodium azide.

Cloning the ATPase from thermophilic Bacillus

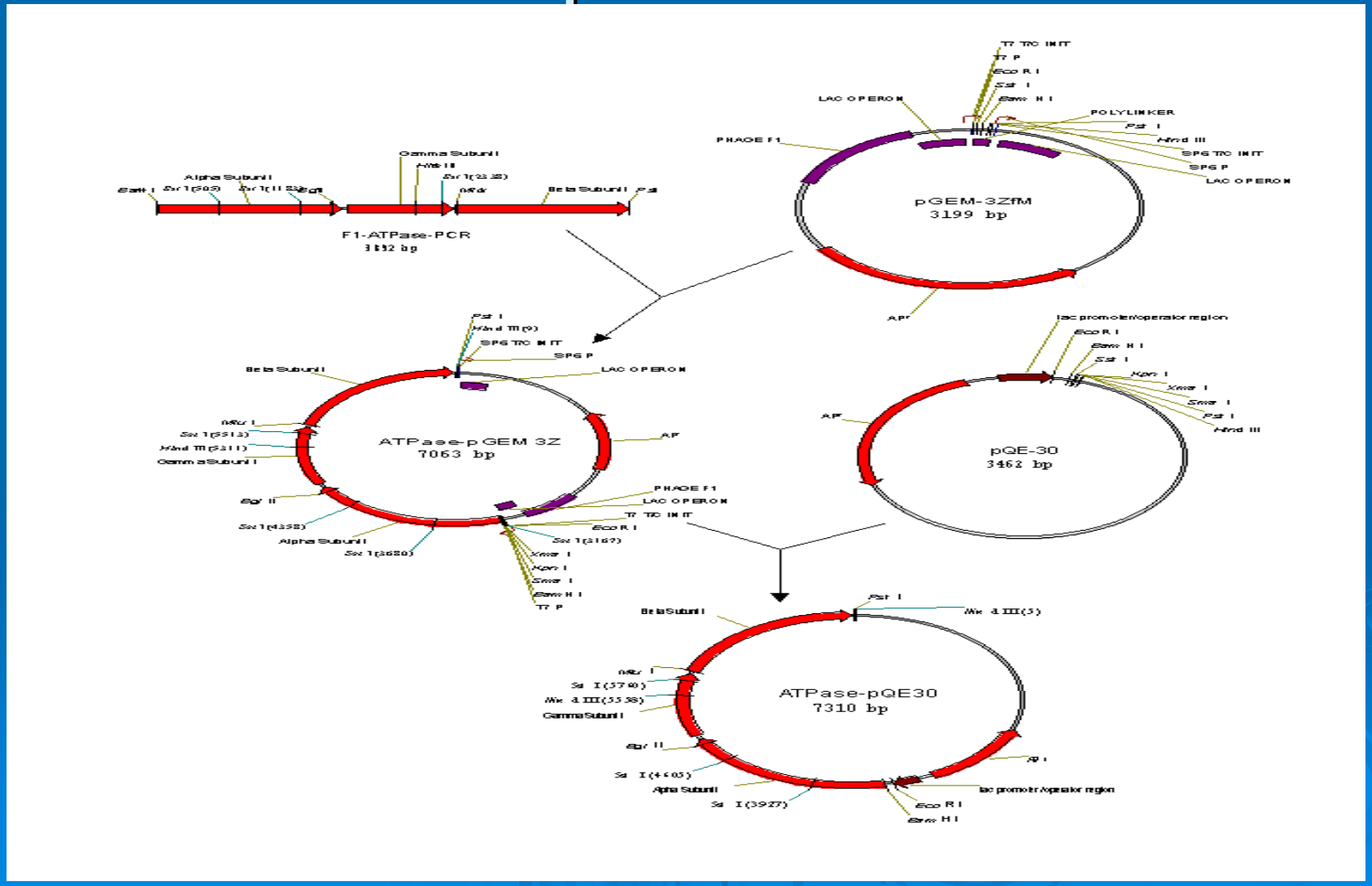

Protein analysis by SDS-PAGE

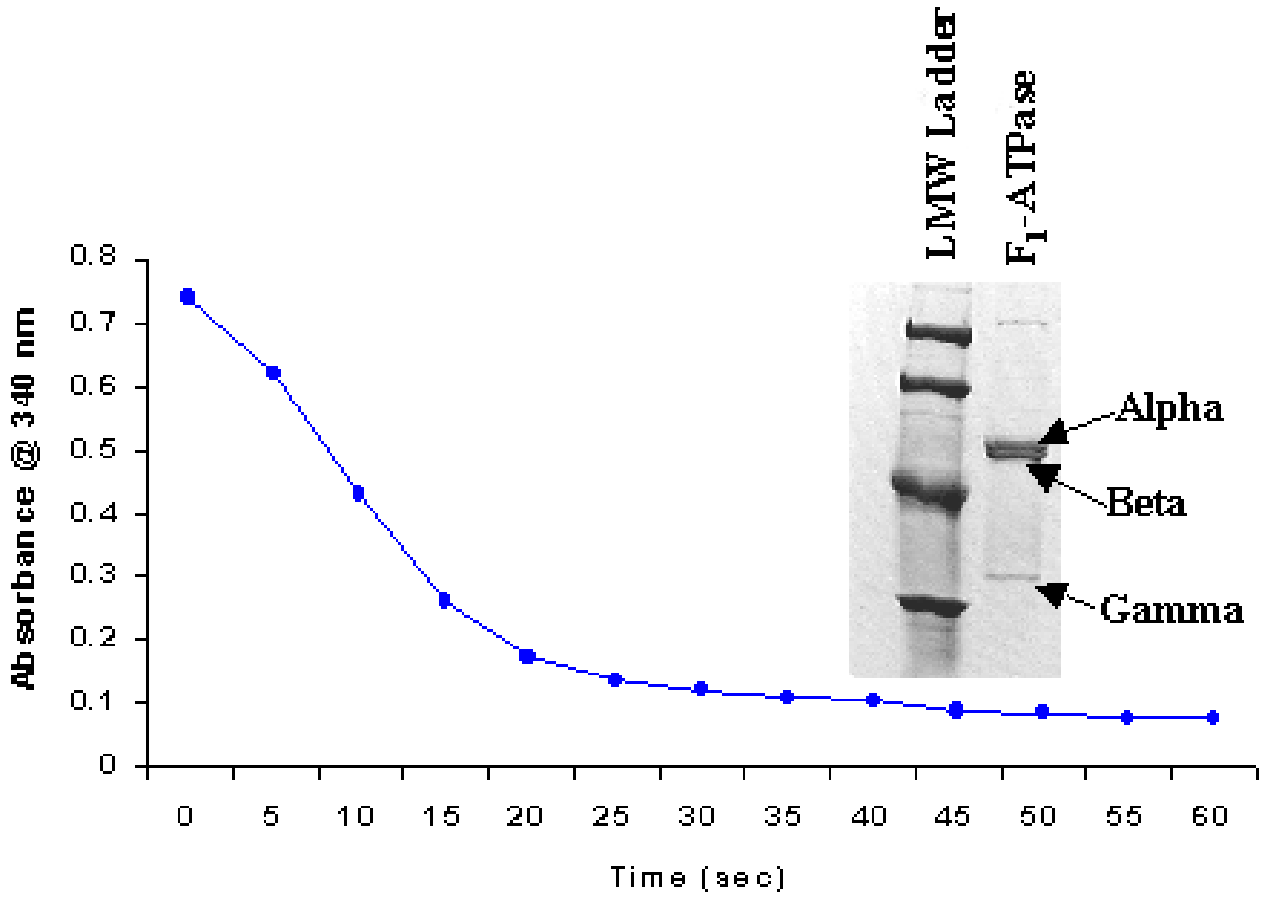

Nanofibricated technology

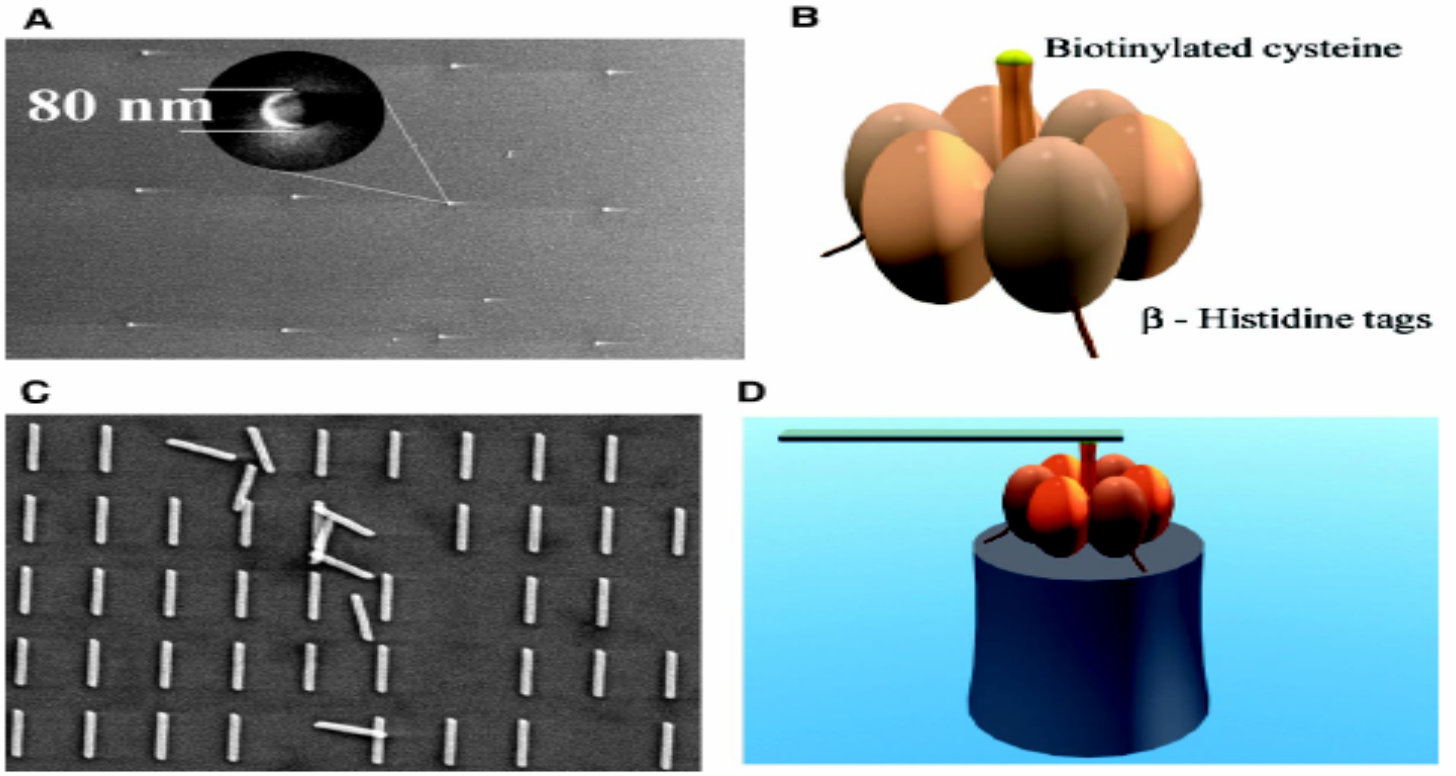

Fig. 1. Schematic diagram of the F_1-ATPase biomolecular motor–powered nanomechanical device. The device consisted of (A) a Ni post (height 200 nm, diameter 80 nm), (B) the F_1-ATPase biomolecular motor, and (C) a nanopropeller (length 750 to 1400 nm, diameter 150 nm). The device (D) was assembled using sequential additions of individual components and differential attachment chemistries.

The assembly of protein and nano-inorganic element

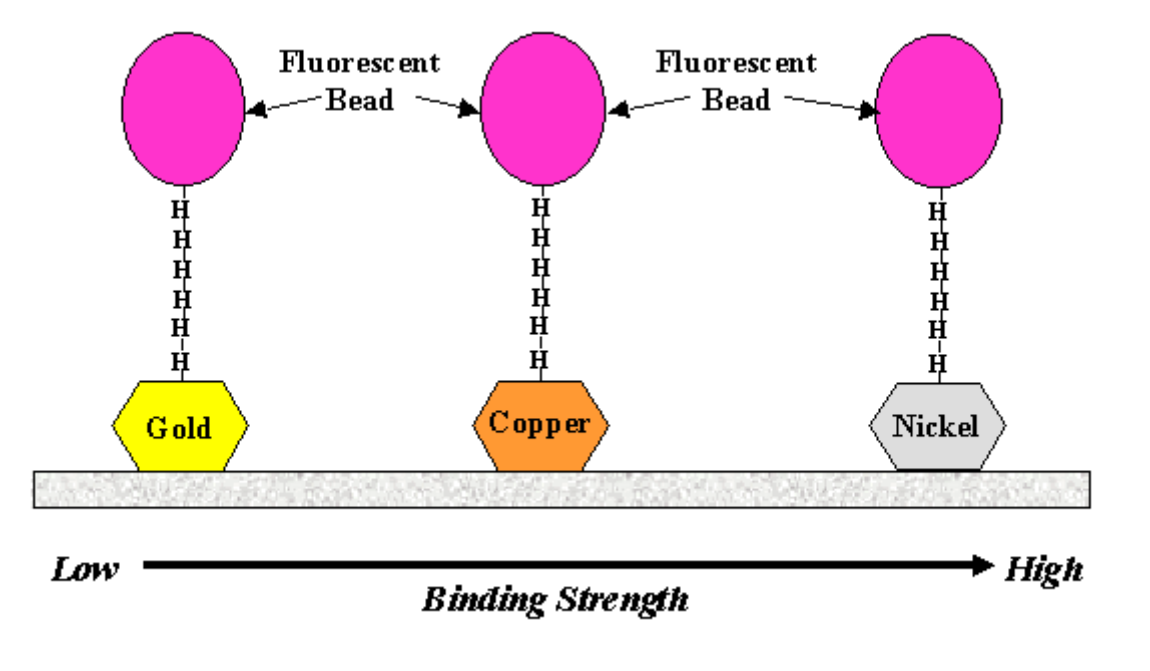

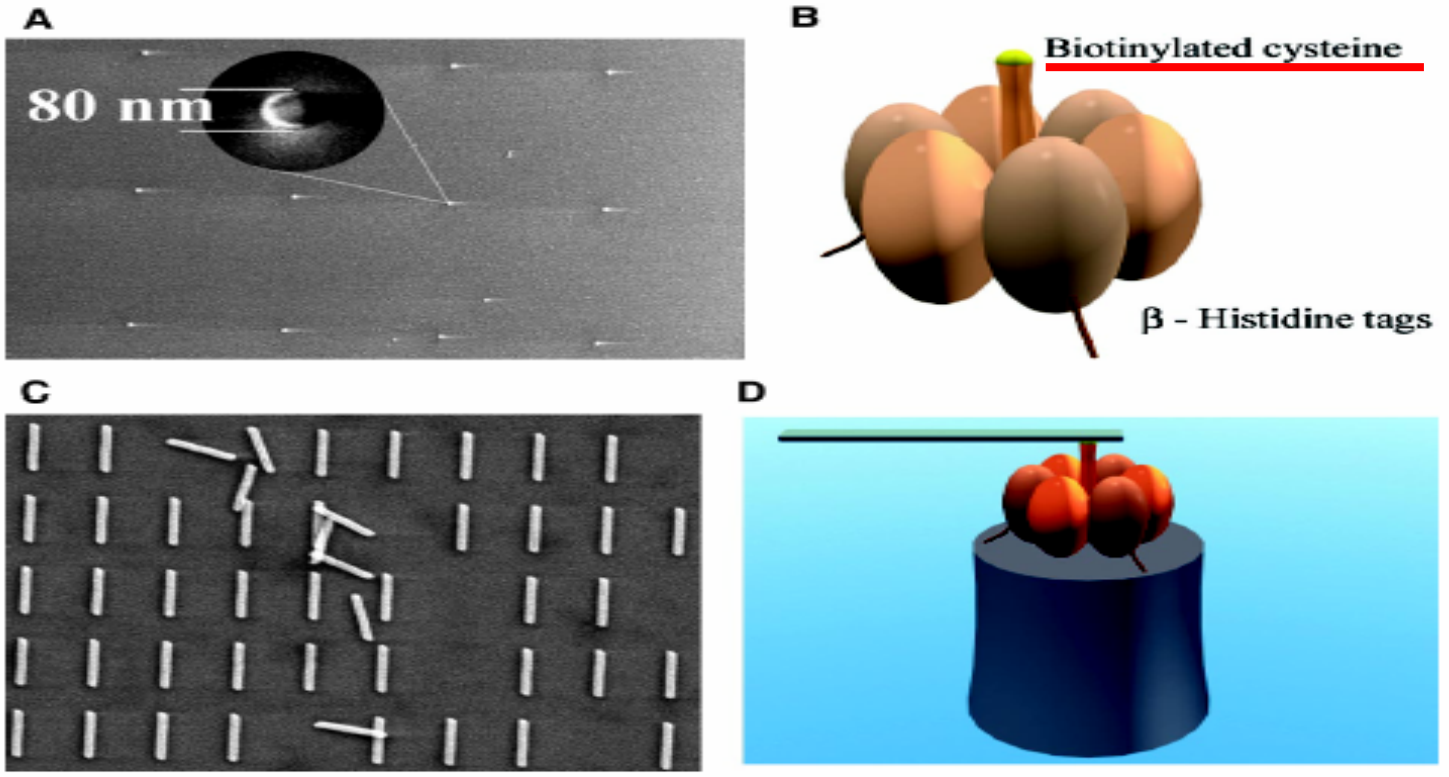

Fig. 1. Schematic diagram of the F_1-ATPase biomolecular motor–powered nanomechanical device. The device consisted of (**A**) a Ni post (height 200 nm, diameter 80 nm), (**B**) the F_1-ATPase biomolecular motor, and (**C**) a nanopropeller (length 750 to 1400 nm, diameter 150 nm). The device (**D**) was assembled using sequential additions of individual components and differential attachment chemistries.

table 7–1

Some Protein Dissociation Constants

Protein	Ligand	K_d (M)*
Avidin (egg white)†	Biotin	1×10^{-15}
Insulin receptor (human)	Insulin	1×10^{-10}
Anti-HIV immunoglobulin (human)‡	gp41 (HIV-1 surface protein)	4×10^{-10}
Nickel-binding protein (*E. coli*)	Ni^{2+}	1×10^{-7}
Calmodulin (rat)§	Ca^{2+}	3×10^{-6}
		2×10^{-5}

*A reported dissociation constant is valid only for the particular solution conditions under which it was measured. K_d values for a protein-ligand interaction can be altered, sometimes by several orders of magnitude, by changes in solution salt concentration, pH, or other variables.

†Interaction of avidin with the enzymatic cofactor biotin is among the strongest noncovalent biochemical interactions known.

‡This immunoglobulin was isolated as part of an effort to develop a vaccine against HIV. Immunoglobulins (described later in the chapter) are highly variable, and the K_d reported here should not be considered characteristic of all immunoglobulins.

§Calmodulin has four binding sites for calcium. The values shown reflect the highest- and lowest-affinity binding sites observed in one set of measurements.

Biotin

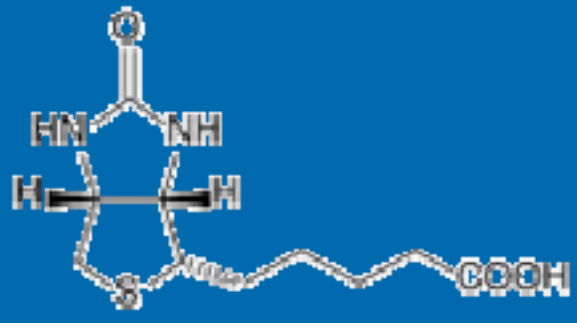

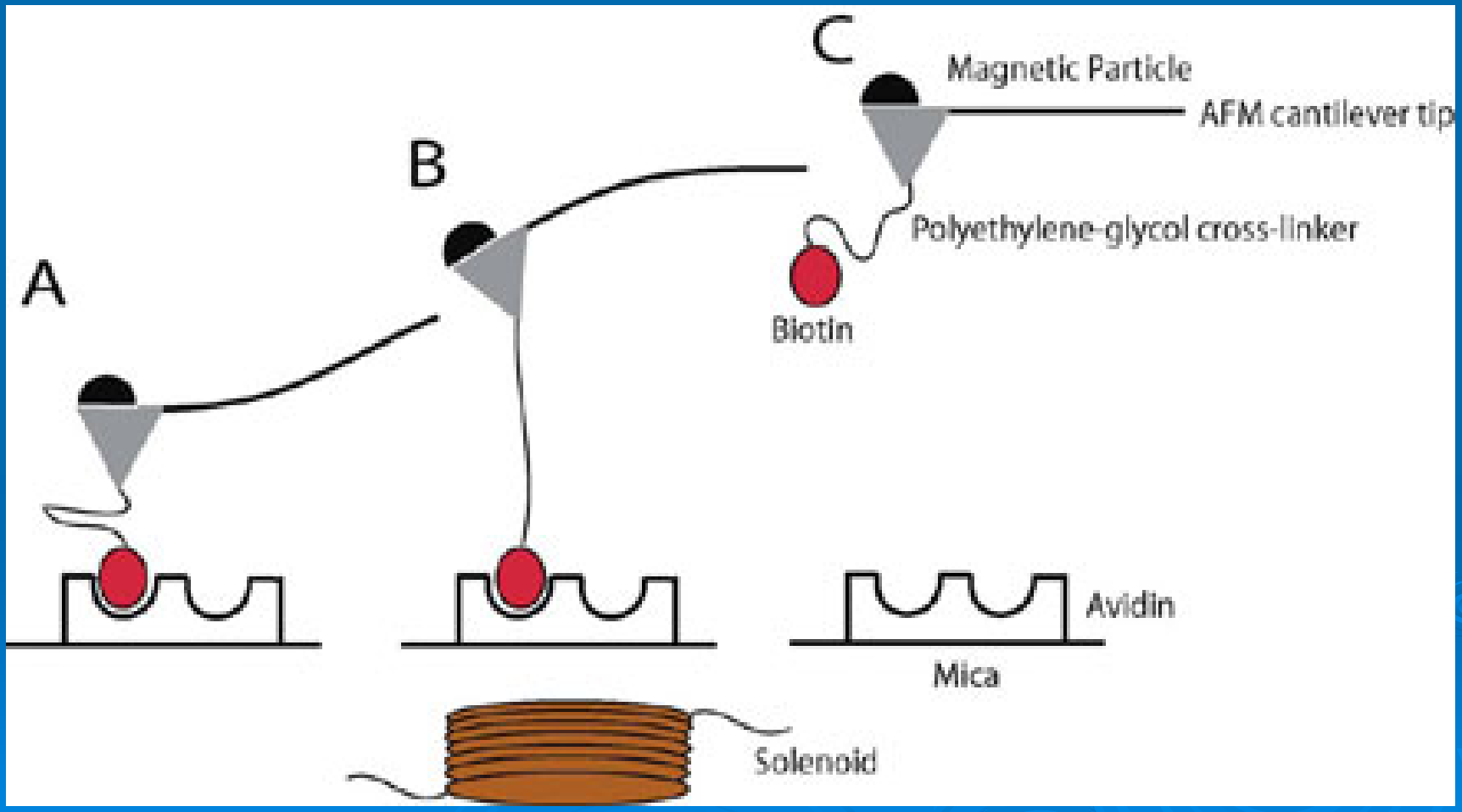

www.nanofunction.org/nano_single_mol.htm

The observation of nanomotor work

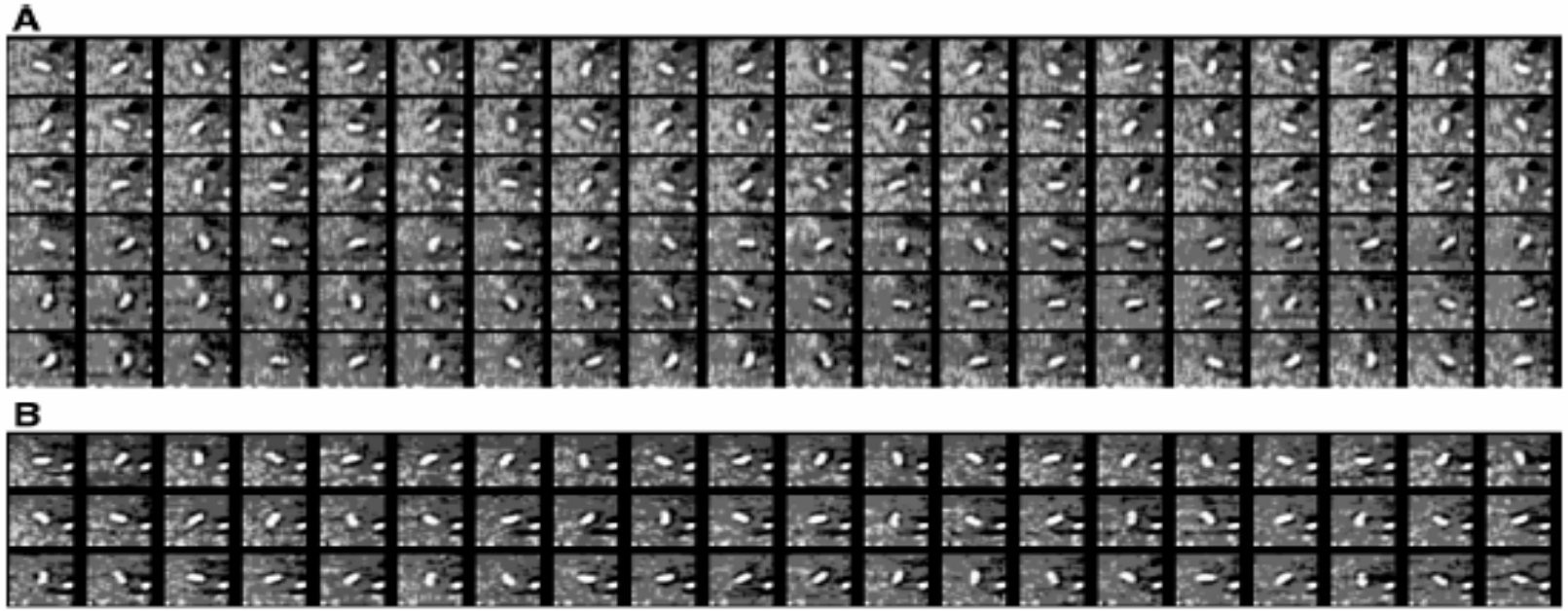

Fig. 2. Image sequence (viewed left to right) of nanopropellers being rotated anticlockwise at 8.3 rps (**A**) and 7.7 rps (**B**) by the F_1-ATPase biomolecular motor. Observations were made using 100× oil immersion or 60× water immersion and were captured with a CCD video camera (frame rate 30 Hz). The rotational velocity ranged from ~0.8 to 8.3 rps, depending on propeller length. Data were recorded for up to 30 min; however, propellers rotated for almost 2.5 hours while ATP was maintained in the flow cell. These sequences can be viewed as movies at the Nanoscale Biological Engineering and Transport Group Web site (http://falcon.aben.cornell.edu/News2.htm).

Fig. 3. Time course of F_1-ATPase γ subunit rotation. Each line represents data from a rotating nanopropeller. Solid lines, propellers 750 nm long; dashed lines, propellers 1400 nm long; dotted lines, propellers 1400 nm long in the presence of NaN_3.

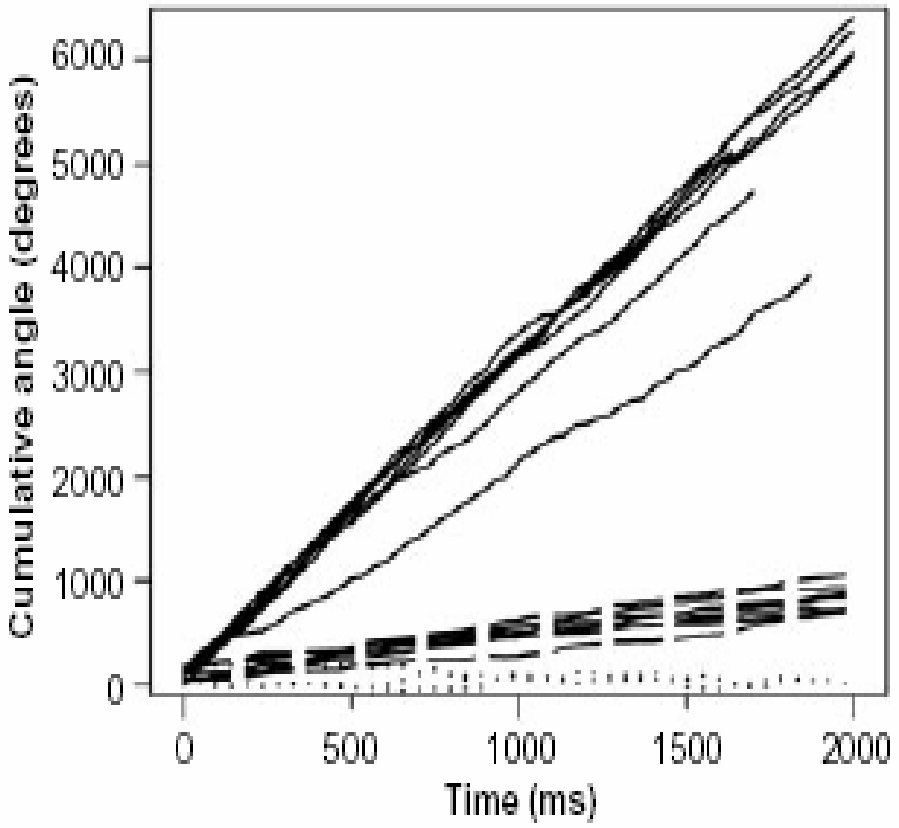

Thanks for your patient

謝謝指教